Transverse Momentum Exchange Induced by Large Coherent Structures in a Vegetated Compound Channel

Truong, S. H.; Uijttewaal, W. S.J.

DOI
10.1029/2018WR023273

Publication date
2019

Document Version
Final published version

Published in
Water Resources Research

Citation (APA)
Truong, S. H., & Uijttewaal, W. S. J. (2019). Transverse Momentum Exchange Induced by Large Coherent Structures in a Vegetated Compound Channel. *Water Resources Research*, *55*(1), 589-612. https://doi.org/10.1029/2018WR023273

Water Resources Research

RESEARCH ARTICLE
10.1029/2018WR023273

Transverse Momentum Exchange Induced by Large Coherent Structures in a Vegetated Compound Channel

S. H. Truong[1,2] **and W. S. J. Uijttewaal**[1]

[1]Hydraulic Department, Faculty of Civil Engineering and Geosciences, Delft University of Technology, Delft, The Netherlands, [2]Hydraulic Department, Faculty of Civil Engineering, Thuy Loi University, Hanoi, Vietnam

Key Points:
- A data set from 39 experimental settings of vegetated compound channel flows was analyzed on the aspect of transverse momentum transfer
- The role of large coherent structures in the process of momentum transfer is revealed
- A new hybrid turbulent viscosity model that includes floodplains, vegetation, and large coherent structures was developed and validated

Supporting Information:
- Supporting Information S1

Correspondence to:
S. H. Truong,
S.TruongHong@tudelft.nl

Citation:
Truong, S. H., & Uijttewaal, W. S. J. (2019). Transverse momentum exchange induced by large coherent structures in a vegetated compound channel. *Water Resources Research*, *55*. https://doi.org/10.1029/2018WR023273

Received 8 MAY 2018
Accepted 2 JAN 2019
Accepted article online 7 JAN 2019

Abstract In floodplains of vegetated channels, transverse exchange processes of mass and momentum are of primary importance as these are directly linked to the river bank stability, sedimentation, and nutrient transport. Despite its importance, knowledge about this phenomenon is still incomplete especially in the context of the presence of the large horizontal coherent structures (LHCSs). As a result, although various exchange models have been developed, their applicability in different circumstances is still unclear as their validity is usually restricted to a narrowly ranging experiment data set. A proper model for this exchange in a compound channel geometry with or without vegetation is lacking. In order to obtain more insight, a laboratory experiment of a shallow flow field in a compound vegetated channel has been conducted. A quadrant analysis of the Reynolds shear stresses has been applied to study the connection between the cycloid flow events induced by the LHCSs and transverse momentum exchange in the channel. It is suggested that local variability leads to differences in the transverse exchange of momentum. Furthermore, the experimental data were used to verify state-of-the-art momentum exchange models. As the limitations of those models were analyzed, for the first time a hybrid eddy viscosity model based on the occurrence of LHCSs and the presence of vegetation was proposed and validated using a variety of experimental data sets. The results suggest that the transverse momentum exchange can be well modeled with the new eddy viscosity model for quite a range of different setups and scenarios by varying only a coefficient of proportionality β, which is related to the transverse slope between the main channel and the floodplain.

1. Introduction

In the Mekong Delta estuaries, mangroves usually dominate the floodplain regions with a gentle slope of about 1:10. Due to the human impacts in many large mangrove forests, only a narrow strip of about 50 to 200 m is left. The river banks at those locations are usually eroding at a rate of 2 to 4 m/year (Figure 1). This degradation of mangrove forests together with the accelerated river bank erosion has been studied in the context of the "squeeze" phenomenon (Phan et al., 2015; Truong et al., 2017). In a squeezed mangrove forest, the presence of lateral tidal creeks is hardly observed and the main interaction is the lateral exchange through the mixing layer developed at the vegetation interface. In this condition, the hydrodynamics of a squeezed estuarine mangrove forest is similar to that of a compound vegetated channel (Mazda et al., 1997; Truong et al., 2017).

A compound channel usually consists of floodplains, transition slopes, and a main open channel. In appropriate conditions, ecological systems such as mangroves or salt marshes can develop in the floodplain region, and the compound channel becomes a compound vegetated channel, also called floodplain vegetated channel. There are also cases in which the channels are partially covered with vegetation and the presence of the floodplain is negligible. The cross sections of these natural channel systems can schematically be depicted, see Figure 2.

In compound channels, the flow over the shallower floodplain is slower than that in the deeper main channel because of the difference in bed friction. As a result, a mixing layer develops between the floodplain and the channel (van Prooijen et al., 2005). A shallow flow field in this condition is considered as a parallel shear flow (Drazin & Reid, 2004) between the floodplain and adjacent open region that can trigger velocity-shear instability, so called the Kelvin-Helmholtz (K-H) instabilities (Bousmar, 2002). The K-H instabilities then

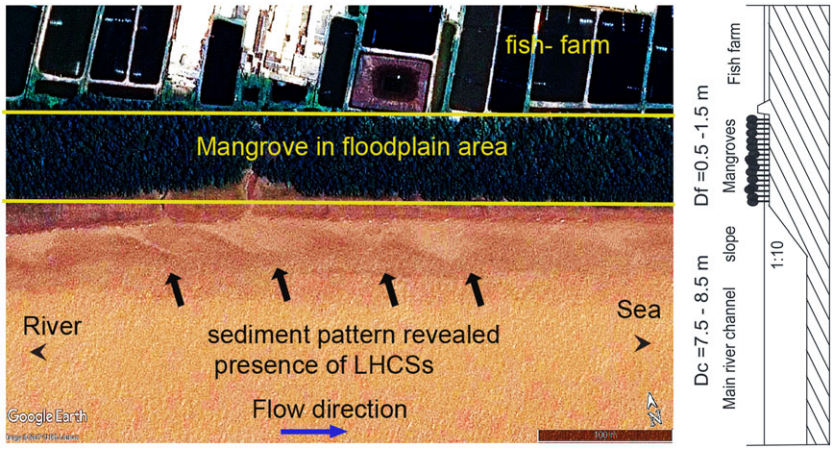

Figure 1. Typical mangroves distribution along a straight part of Tieu estuary, Vietnam, and the associated schematized bathymetry. Fish farms constructed close to the water boundary push the mangrove into a narrow fringe zone. This area is suffering from erosion with a rate of about 2.5 m/year (Truong et al., 2017).

induces the flow to develop a kind of self-organizing flow structures with horizontal length scale larger than the water depth, which is termed "large horizontal coherent flow structures" (LHCSs) (Adrian & Marusic, 2012; Bousmar, 2002; White & Nepf, 2008). It is considered to be the fundamental factor controlling the structure of these turbulent flows. The presence of LHCSs was well observed not only at the interface of open compound channel but also in cases of flow past river groynes (Talstra, 2011), the confluence of two flows (Uijttewaal & Booij, 2000; van Prooijen, 2004; van Prooijen et al., 2005), in the wakes of islands (Chen & Jirka, 1997), along the edge of vegetation (Nezu et al., 1999; Nezu & Sanjou, 2008). They usually appear in the mixing layer, where there is a large gradient in velocities.

In cases of shallow water over a flat bottom, the bottom friction affects the mixing layer and LHCSs as it decreases the velocity differences and the growth of K-H instability downstream (Uijttewaal & Booij, 2000). However, in compound channels, the transverse depth difference sustains the velocity difference and the bed friction limits the growth of the mixing layer. Consequently, the mixing layer can achieve an equilibrium width and the flow field is fully developed after a certain width, for example, 7.5 m in cases of a compound channel profile (Fernandes et al., 2014) and 4 m in cases of a partially vegetated channel profile (White & Nepf, 2007). As a result, the presence of LHCSs can be sustained in this fully developed region.

In a vegetated compound channel, a similar shear layer is generated. However, the presence of vegetation adds to friction, turbulence, and drag forces, greatly damping the flow in this region, and significantly boosting the magnitude of the velocity gradient between the vegetation and open channel region (White & Nepf, 2007, 2008). As a result, the K-H instabilities increase and the LHCSs formed at the vegetation interface, observed in floodplain vegetated channels are more pronounced than in cases without vegetation. These pronounced LHCSs then promote more transverse momentum exchange into the vegetation region (Nepf, 1999). The transverse exchange of momentum from "fast" regions to "slow" regions, mediated by the strong presence of the LHCSs is the major interest of this study.

2. Objectives

In recent decades, numerous studies on compound channels have been published, particularly focusing on understanding and quantifying the lateral momentum exchange processes in the mixing layer of a

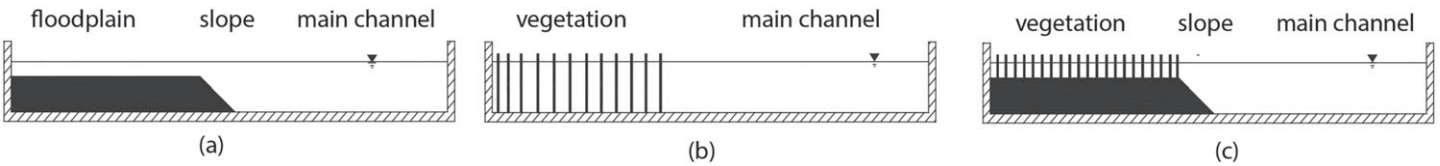

Figure 2. Typical schematized profiles of natural systems of a straight river channel including compound channel (a), partially vegetated channel (b), and vegetated floodplain channel (c).

compound channel, with or without vegetation (Helmiö, 2004; Ikeda et al., 1991; Nadaoka & Yagi, 1998; Nezu & Onitsuka, 2001; Pasche & Rouve, 1985; Tamai et al., 1986; van Prooijen et al., 2005; Vionnet et al., 2004; White & Nepf, 2007, 2008; Xiaohui & Li, 2002; Zong & Nepf, 2010). However, these studies either did not take into account the presence of LHCSs or the presence of the vegetation on the floodplain. Furthermore, those models have primarily been based on laboratory studies, and each model refers to a particular setup. It has not yet been determined whether or not they are broadly valid for different configurations and scales. It is unclear how and to what extent the presence of the LHCSs affects the flow field and the transverse exchange of momentum of a compound vegetated channel. Therefore, the main objectives of this research are as follows: (1) to obtain insight into the transverse momentum exchange in the shallow flow field between the open channel and the vegetated region induced by the LHCSs and (2) to verify and extend the momentum exchange model for compound vegetated channels based on the effective eddy viscosity model of van Prooijen et al. (2005).

3. Methodology

Momentum exchange in a compound channel flow can be expressed as a turbulent shear stress ($\overline{u'\ v'}$) or using the concept of an eddy viscosity (ν_t): $\tau_{xy} \approx -\rho\cdot\overline{u'\ v'} \approx -\rho\cdot\upsilon_t\cdot\frac{\partial u}{\partial y}$ (van Prooijen et al., 2005). While the former is important for understanding the mechanisms contributing to the transverse exchange of momentum, the latter plays a key role in modeling it. Both aspects are addressed in this study.

The governing equations are introduced (section 4), and existing modeling approaches of transverse exchange of momentum are reviewed (section 5). A laboratory study was chosen as a major source of data (section 6). Subsequently, a quadrant analysis of the Reynolds shear stress is applied (section 7). Then, a hybrid model of the eddy viscosity (υ_t) is proposed (section 8). The model is then verified using 39 different experimental settings (section 9), including the experiments of the current study (Table A1 in the appendix), three representative cases of White and Nepf (2007) for partially vegetated channels, and the experimental results of Lambert and Sellin (1996) and Ervine et al. (2000), which were also used to validate the effective eddy viscosity model of van Prooijen et al. (2005). Finally, conclusions are drawn in section 10.

4. Governing Equations

In compound vegetated channels (Figure 2c), near a porous vegetation interface, the equations of fully developed stationary flow motion can be derived by applying the time-averaged, spatially averaged, and depth-averaged properties to the 2-D shallow water equations, which is similar to that used by White and Nepf (2007) for partially vegetated channels. In this way, a simplified momentum exchange equation for the floodplain vegetated channel, with streamwise uniform flows can be written as:

$$0 = -g\ D\ \frac{\partial n\zeta}{\partial x} + \frac{1}{\rho}\ \frac{\partial nD\left\langle \overline{T_{xy}} \right\rangle_d}{\partial y} -\ D\cdot D_x \tag{1}$$

In which

- $D\ =\ D(y)$ is the water depth, $D\cdot D_x$ is the drag force exerted on the fluid in the x (streamwise direction).
- n is porosity, ρ is mass density, and ζ is water level above an arbitrary horizontal reference plane.
- The term $\frac{1}{\rho}\ \frac{\partial nD\left\langle \overline{T_{xy}} \right\rangle_d}{\partial y}$ accounts for the transverse exchange of streamwise momentum between the open channel and the vegetated floodplain regions.
- $\left\langle \overline{T_{xy}} \right\rangle_d$ is the sum of depth, time, and space averaged transverse shear stress.
- The term $-g\ D\ \frac{\partial n\zeta}{\partial x} - D\cdot D_x$ is the difference of the flow from an equilibrium channel flow without transverse exchange (due to slope and vegetation).
- $\frac{\partial n\zeta}{\partial x}$ is the pressure gradient term.
- D_x is drag force exerted on the fluid in the x direction (streamwise direction), where

$$D_x = \begin{cases} \frac{1}{2}\ \langle \overline{u} \rangle_d^2 \left(\frac{C_f}{D} + C_D\cdot a \right) & y < 0 \quad \text{“in vegetation”} \\ \frac{1}{2}\ \langle \overline{u} \rangle_d^2 \left(\frac{C_f}{D} \right) & y > 0 \quad \text{“no vegetation”} \end{cases} \tag{2}$$

Where

- C_f is the Bed friction coefficient.
- C_d is the drag coefficient of the array element.
- a is the average solid frontal area per unit volume in the plane perpendicular to the flow (White & Nepf, 2007), $a = N \cdot d$, where N is the density of cylinders (cylinder area) and d is the cylinder diameter.

In cases of high Reynolds numbers, the contribution of viscous stress ($\mu \frac{\partial U}{\partial y}$) is small compared to depth-averaged Reynolds stress. Thus, the viscous term has been neglected in these equations. It is noticed that this momentum equation can be globally applied to study the transverse momentum exchange in various scenarios of constant depth or with different depth along the channel (in the presence of the floodplain) and with or without vegetation. In cases of a partially vegetated channel (of constant depth; Figure 2b), equation (1) reduces to

$$0 = -g\,\frac{\partial n\zeta}{\partial x} + \frac{1}{\rho}\,\frac{\partial n\left\langle \overline{T_{xy}} \right\rangle_d}{\partial y} - D_x \tag{3}$$

In cases of a nonvegetated floodplain ($Cda = 0$; Figure 2a), due to the absence of vegetation, equation (1) reduces to

$$0 = -g\,D\,\frac{\partial \zeta}{\partial x} + \frac{1}{\rho}\,\frac{\partial D\overline{T_{xy_d}}}{\partial y} - D \cdot D_x \tag{4}$$

Equation (3) was studied by White and Nepf (2007). It was applied to different regions of the channel, finding separate scaling of the inner and outer layers of the mixing layer in a partially vegetated channel (Figure 2b). Equation (4) was studied by van Prooijen et al. (2005). They proposed a constant mixing length across the compound channel and studied the mixing layer as a whole (Figure 2a). These two equations are special cases of equation (1). In floodplain vegetated channels (Figure 2c), due to the presence of both the floodplain and the vegetation, equation (1) needs to be considered in which the time- and depth-averaged transverse shear stress or so-called transverse exchange of downstream momentum ($\left\langle \overline{T_{xy}} \right\rangle_d$) is the most significant term left that needs to be modeled. It is the sum of time-, space-, and depth-averaged transverse shear stress due to advective dispersion, turbulence, and viscosity, respectively,

$$\left\langle \overline{T_{xy}} \right\rangle_d = -\rho \left\langle \left(\langle \overline{u} \rangle - \langle \overline{u} \rangle_d \right) \left(\langle \overline{v} \rangle - \langle \overline{v} \rangle_d \right) \right\rangle_d - \rho \left\langle \overline{u'\,v'} \right\rangle_d - \rho \left\langle \overline{u''\,v''} \right\rangle_d, \tag{5}$$

where

- $\langle \overline{u} \rangle_d, \langle \overline{v} \rangle_d$ are time-averaged, spatially averaged, and depth-averaged streamwise and transverse velocities.
- u', v' are streamwise and transverse velocity temporal fluctuations, $u' = u - \overline{u}$, $v' = v - \overline{v}$.
- u'', v'' are streamwise and transverse velocity spatial fluctuations, $u'' = \overline{u} - \langle \overline{u} \rangle$, $v'' = \overline{v} - \langle \overline{v} \rangle$.
- $-\rho \left\langle \left(\langle \overline{u} \rangle - \langle \overline{u} \rangle_d \right) \left(\langle \overline{v} \rangle - \langle \overline{v} \rangle_d \right) \right\rangle_d$ are advective dispersion stresses due to depth variation in the mean flow, $-\rho \left\langle \overline{u'\,v'} \right\rangle_d$ is Turbulent Reynolds stresses and $-\rho \left\langle \overline{u''\,v''} \right\rangle_d$ is dispersive stress due to spatial fluctuations.

For flow through and around vegetated regions, at high Reynolds number, the Reynolds stress is the main shear stress. Since the stress that contributed from secondary circulations is for most conditions small (van Prooijen et al., 2005) and for the dense arrays, $ad > 0.01$ (Poggi, Katul, and Albertson, 2004; Poggi, Porporato, et al., 2004) dispersive stresses are also relatively small. So the time-averaged, spatially averaged, and depth-averaged Reynolds shear stress are assumed to account for the total momentum exchange between the open channel and vegetated floodplain area. This means that:

$$\left\langle \overline{T_{xy}} \right\rangle_d \approx -\rho \left\langle \overline{u'\,v'} \right\rangle_d \tag{6}$$

The eddy viscosity concept or Boussinesq approach is usually used to model this turbulent shear stress:

$$\left\langle \overline{T_{xy}} \right\rangle_d \approx -\rho \left\langle \overline{u'\,v'} \right\rangle_d = \nu_t\,\frac{\mathrm{d}\langle \overline{u} \rangle_d}{\mathrm{d}y} \tag{7}$$

In this sense, the determination of the transverse exchange of momentum is replaced by the finding of a proper eddy viscosity (ν_t) model.

Table 1
Two Insightful Models for the Transverse Exchange of Streamwise Momentum

Model concept	Author	$T_{xy} \approx -\rho \cdot \upsilon_t \cdot \frac{\partial u}{\partial y}$	Note
Effective eddy viscosity concept	van Prooijen et al. (2005)	$\upsilon_t = \alpha\sqrt{c_f}\langle\overline{u}\rangle_d D + \frac{Dm}{D(y)}\beta^2\delta^2\left\lvert\frac{\mathrm{d}\langle u\rangle_d}{\mathrm{d}}y\right\rvert$	$\alpha = 0.1$ $\beta = 0.07$
Vortex based model	White and Nepf (2008)	$\upsilon_{t\_\mathrm{outer}} = 0.7 \cdot u_*^2 \cdot \frac{\delta_2}{U_c} - U_m$ $\upsilon_{t\_\mathrm{inner}} = u_*^2 \cdot \frac{\delta_1}{U_0 - U_f}$	$U_m = U(y_m)$

5. Existing Models of Transverse Exchange of Momentum

As quoted in previous sections, numerous momentum exchange models have been developed, in which the LHCSs have been considered as a fundamental element in the lateral momentum exchange between the slow flow and fast flow regions (Nadaoka & Yagi, 1998; Nezu & Onitsuka, 2001; Tamai et al., 1986; Uijttewaal & Booij, 2000; Xiaohui & Li, 2002; van Prooijen et al., 2005; White & Nepf, 2007, 2008; Zong & Nepf, 2010). However, it is not our main aim to discuss all of those here, only the most recent two insightful models of van Prooijen et al. (2005) and White and Nepf (2008) are chosen to be discussed (Table 1). While the former was developed for the unvegetated compound channels, the latter is the most up-to-date model developed for the partially vegetated channel without considering the lateral depth variations.

The transverse momentum exchange model, proposed by van Prooijen et al. (2005) including the physics of the LHCSs, appears to be one of the most insightful models for the compound channel without vegetation. In that model, the contribution from the LHCSs and bottom turbulence, as well as the effect of transverse depth variation are considered. Nevertheless, there is no vegetation and the mean streamwise velocity gradient is only caused by the shallowness due to the floodplain region. Consequently, in scenarios with vegetation, the model cannot capture the significant reduction in the turbulent length scale due to the high resistance from vegetation and may overestimate the penetration of the flow into the vegetation region (White & Nepf, 2008).

By dividing the mixing layer into different layers (inner layer δ_1, and outer layer δ_2), each has its own length scale and is connected by the matching point (y_m) where continuity of the velocity profile is required, a vortex-based model had been proposed by White and Nepf (2008). That model allows to estimate the maximum penetration of the mixing layer into the cylinder arrays and is considered to be the most advanced model for the channel with partial vegetation. It is also suggested that the penetration scale of the momentum into the vegetation region mainly depends on the vegetation characteristic (or $C_d a$). Other effects are minor and can be neglected. However, in that study, the floodplain was not considered. This means that the shallowness or water depth variations have not been taken into account. The velocity gradient and corresponding LHCSs are only caused by the resistance from the presence of vegetation. As mentioned in previous sections, the vegetated channel without floodplain is only a special case of floodplain vegetated channels with depth ratio equal to 1 ($D_r = D_f/D_c = 1$). Neglecting the presence of a floodplain may significantly affect the physical exchange processes. In this sense, which of these models is suitable for a vegetated floodplain channel is yet to be determined.

6. Experiment Setup and General Results

An experiment was conducted in the shallow, free-surface flow facility of the Fluid Mechanics Laboratory at the Delft University of Technology. A top view and a cross section of the experimental setup and some flow features observed during the experiment are shown in Figure 3. A Nortek Acoustic Dopper Velocity meter (ADV) was used to measure the mean streamwise velocity at a sampling rate of 25 Hz. Particle Image Velocimetry (PIV) was applied to measure the instantaneous movement of flow at 10 Hz over a domain of 2 $\times$ 2 m^2 using 3 mm floating particles. The detailed experimental configurations and parameters are provided in the appendix.

In this study, the main data set is the time series of the streamwise velocity $U(y)$ and lateral velocity $V(y)$ at a cross section, obtained from an ADV. This data set was used to determine the transverse momentum exchange between the main channel and floodplain in a compound channel with a gentle slope. The ADV was placed at 10 m downstream from the floodplain starting point (5 m from the first row of cylinder) where

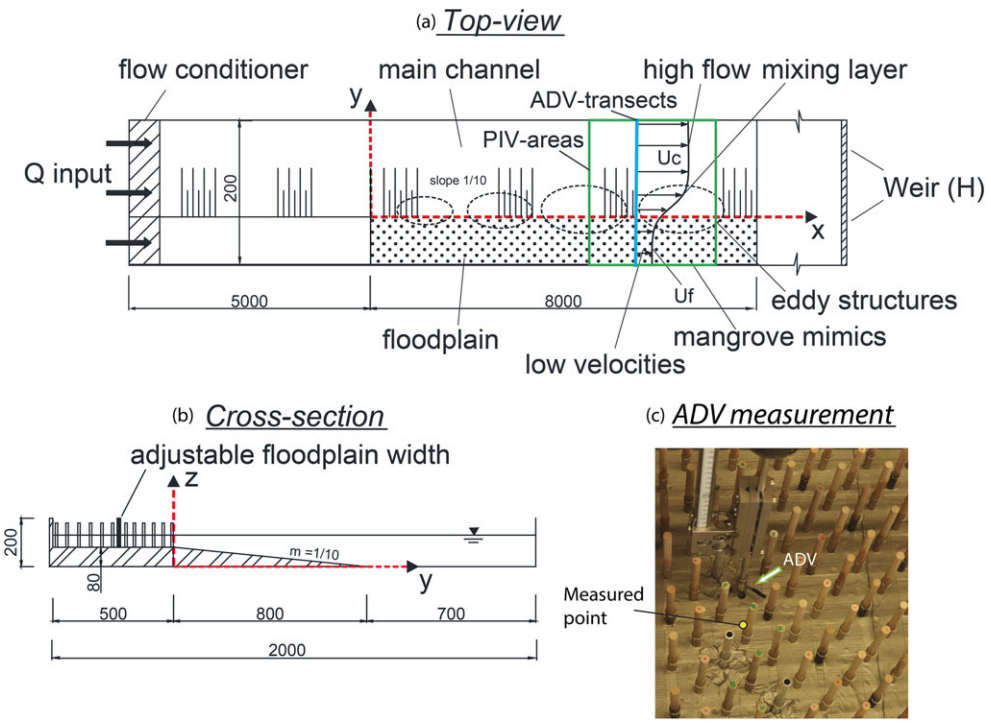

Figure 3. Schematic view of the experiment setup (units in millimeter), the presence of large coherent structures in the flow field. Top view (a), cross section (b), a middepth velocity measurement using ADV inside the vegetation (c). Not to scale.

a fully developed flow field can be achieved (Uijttewaal & Booij, 2000; White & Nepf, 2007). At this location, the flow field was checked to be fully developed (see Figure A1 in the appendix). In order to capture a velocity profile over the cross section, at least 20 points were taken at the middepth. Middepth measurements means that the distance from the measurement point to the bed changes with flow depth across the lateral profile.

Figure 3c illustrates how a middepth mean streamwise velocity was measured by the ADV inside the vegetation. A cylinder was replaced by the ADV. Furthermore, the exact measured point locates about 5 cm in front of the head of the ADV measurement and thereby in the middle of the cylinder arrays. In this way, the influences of the ADV on the surrounding flow as well as the effects of vortex shedding phenomenon on the measured velocity signal can be reduced.

Figure 4 illustrates the represenative experimental results. It is suggested that the increased drag due to vegetation can substantially reduce the local flow velocity, thereby increasing the velocity gradient between the adjacent open channel and the vegetation region, withdrawing more momentum toward the floodplain vegetated region (see Figures 4a and 4b).

As the LHCSs move along the vegetation interface, they generate cycloid flow events, which are composed of sweeps, ejections, stagnant, and reverse flows. These flow events then divide the shallow flow field of a vegetated compound channel with a gentle slope into three main different regions, which are driven by different physical parameters and have different length scales (Figure 4). The uniform region in the main channel (region II) is controlled by the bottom friction (C_f), the corresponding length scale is the water depth (D_c). The uniform region inside the floodplain (region I) is controlled by drag force ($C_d \cdot a$) from the vegetation. The relevant length scales are the cylinder diameter (d) and the distance between cylinders (s), and the water depth (D_f). In between these regions the mixing layer (regions III and IV),is governed by the LHCSs. The corresponding length scales in this region are the width of the penetration into the vegetation (δ_1), the outer layer width (δ_2), and the water depth ($D(y)$). The presence of LHCSs is the key factor in the mixing layer determining the transverse exchange of momentum between the open regions (II, IV) and the vegetated regions (I, III).

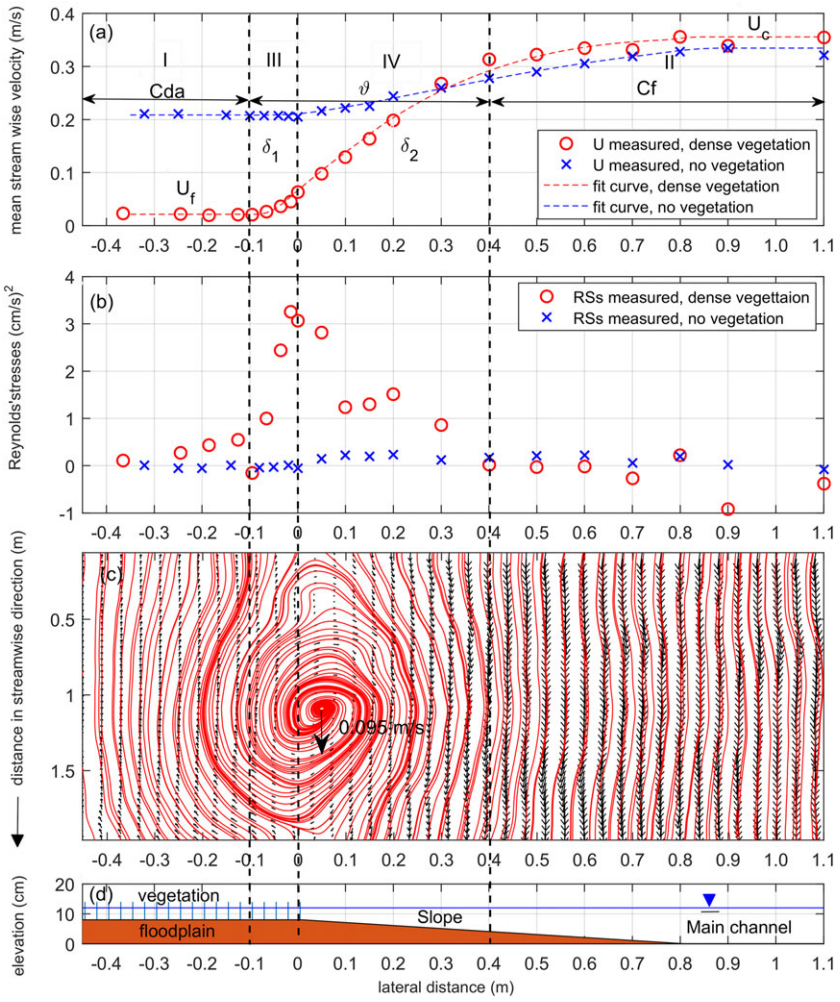

Figure 4. Representative mean streamwise velocity (a) and Reynold shear stresses (b) in cases with and without vegetation. The representative large horizontal coherent flow structures captured through the streamlines of the instantaneous fluctuating velocity field and its corresponding effect on the mean streamwise velocity (c). Corresponding profile of a vegetated compound channel with a gentle slope (d). Dense scenario, 50-cm floodplain width, discharge = 45 L/s, water depth =12 cm. The vegetated floodplain starts from $y = 0$ in the negative direction.

7. Quadrant Analysis of the Cycloid Flow Field Under the Effects of LHCSs

A quadrant analysis of the Reynolds shear stress is a simple but useful turbulence data processing technique that is able to provide insightful information on the contribution to the turbulent shear stress from various events in the flows (Kim et al., 1987; Wallace et al., 1972; Willmarth & Lu, 1972). This quadrant analysis technique can also be used to study the organized structures in the channel flow (Kim & Moin, 1986). In this section of the paper, the quadrant analysis of the Reynolds shear stresses (RSs) was performed to examine the connection between the motion of the LHCSs and the associated cycloid flow events as well as their contribution to the total transverse exchange of momentum.

Figure 5a illustrates the power density spectra (PDSs) of the lateral fluctuation velocity v' at different locations of the cross section. It can be clearly seen that in the high-frequency regions of the PDSs at a location in the main channel ($y = 1.1$ m), the decrease in energy density almost follows a slope $-5/3$ that is indicative of flows with a large inertial subrange. However, inside the vegetation ($y = -0.245, -0.125, -0.015$ m) the decrease of the energy density does not properly follow this rule. The presence of vegetation is likely to affect the energy cascade, as large turbulence structures are more quickly transformed into smaller scale turbulent structures. Additionally, the Reynolds number in this region is not so high (in the range of 1,000 to 7,500) that a large inertial range is formed. Furthermore, the large-scale structures make the flow to vary over time

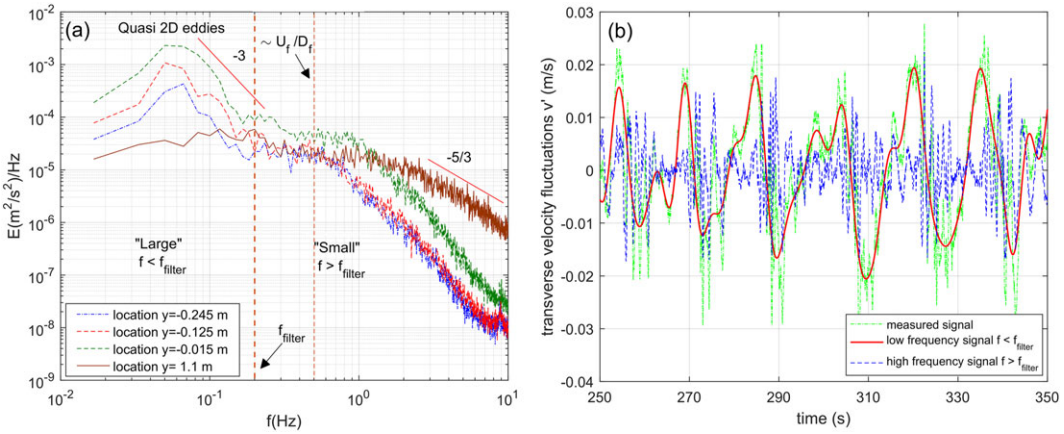

Figure 5. (a) Representative power spectral density at different locations along the cross section. (b) Separation of the "large" and "small" transverse velocity signal by using a filter frequency ($f_{\text{filter}} = 0.2$ Hz), location $y = -0.125$ m for dense scenarios. Case of dense vegetation, floodplain width $H = 50$ cm, discharge $Q = 45$ L/s, and water level $H = 12$ cm.

scales larger than the time scale of the 3-D turbulence. These interactions are likely to cause deviations from the standard Kolmogorov spectrum.

The power density spectra of the transverse fluctuation velocity show definite peaks with a −3 slope corresponding to the quasi 2-D large horizontal coherent structures ($f < f_{\text{filter}} = 0.2$ Hz; Uijttewaal & Booij, 2000). These peak regions are associated with the low-frequencies signals (LHCSs) and were separated from the high-frequencies signals (Figure 5b) using a low-pass filter defining the low frequencies ($f < f_{\text{filter}}$) and the high frequencies ($f > f_{\text{filter}}$). In this way, the RSs induced by LHCSs (low-frequency signal) can be filtered and compared with the total RSs (Figure 6).

Results confirm the dominant contribution of the LHCSs to the total turbulent shear stress. For instance, at the edge of the floodplain vegetated region, RSs induced by LHCSs contribute more than 90% to the total the RSs. It is noticed that there is a significant decrease in the value of the RSs at location $y = -0.1m$ which can be interpreted as the distance of the penetration of the LHCSs into the vegetation area. The remarkable result for y= 0.9 m is most likely related to the transition from the sloped bed to the horizontal bed, providing a different role for the smaller scales compared to the large scales. It is noted that the absolute value of RSs induced by the LHCSs ($f < f_{filter}$) may be larger than the absolute value of the total RSs. This means that small scale motions in the flow are correlated differently and thereby may reduce the Reynold shear stress induced by large scale motions. A quadrant analysis of the turbulent fluctuations will therefore shed more light on this behavior.

The separate low-frequency signals are plotted in the quadrants together with the original measured signals (Figures 7a to 7d). In this way, the contribution of LHCSs and their associated flow events to the total turbulent stresses can be clearly apprehended. Figure 7 shows results for different locations in the cross sections of the vegetated compound channel; from the vegetated floodplain edge (a) to inside the vegetation (c) and in the main open channel (d). According to the sign of u' and v', the quadrant analysis divides the RSs into four quadrants (I-Q1, II-Q2, III-Q3, and IV-Q4).

These four quadrants are associated with four different events, namely outward interactions ($u' > 0, v' > 0$), ejections ($u' < 0, v' > 0$), inward interactions ($u' < 0, v' < 0$), and sweeps ($u' > 0, v' < 0$), respectively. While the Q2 and Q4 motions, which are related to the ejection and sweep events can be clearly visualized, the Q1 and Q3 motions, which are linked to the outward and inward interactions are lacking a descriptive terminology and are less obviously visualized (Wallace, 2016).

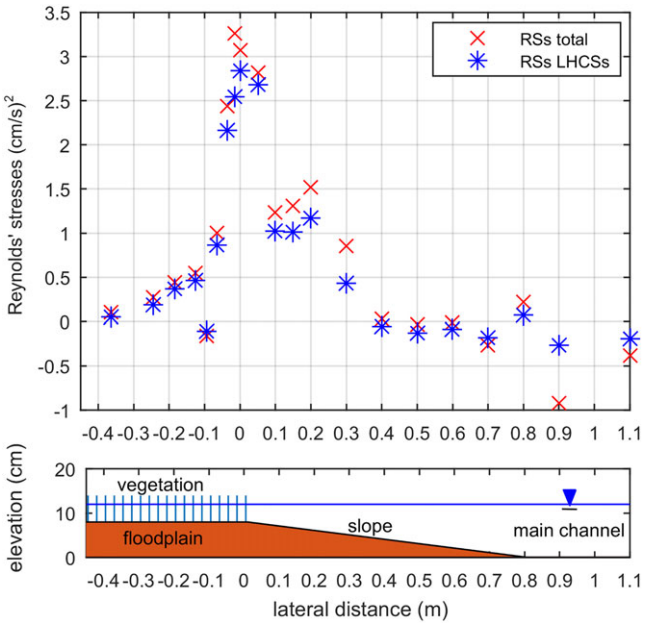

Figure 6. Reynolds shear stresses (RSs) induced by the large horizontal coherent flow structures (LHCSs) compared to total RSs in the case of dense vegetation, floodplain width $H = 50$ cm, discharge $Q = 45$ l/s and water level $H = 12$ cm.

It is clear that the distribution in the quadrants of flow events associated with the LHCSs (low-frequency signals) are different from the floodplain edge toward the region inside the vegetation. At the edge of the vegetated floodplain (Figure 7a) the distribution of (u', v') corresponding to the "large" structures is mainly found in Q2 and Q4. This means that the dominant events are the ejection (Q2) and the sweep (Q4) implying that the exchange of momentum happens strongest at the edge of the floodplain, mediated by sweeps and ejections. This result is also in line with the observations in the partially vegetated channel of (White & Nepf, 2007, 2008). However, deeper inside the vegetation (Figures 7b and 7c), the contributions of the signal in Q2 and Q4 become smaller, and those in Q1 and Q3 larger. This means that the momentum exchange at these locations or the effect of LHCSs is smaller. In the main channel (Figure 7d), as there is no LHCSs at this location, the presence of LHCSs associated with sweep and ejection events cannot be observed. Although there are many events associated with large $u'v'$, their average is almost zero which implies that there is virtually no transverse momentum exchange at this location.

8. Modeling Transverse Momentum Exchange in Vegetated Floodplain Channel

As described in previous sections, the total momentum exchange between the open channel and vegetated floodplain area is mainly represented by the time-averaged, depth-averaged, and spatially averaged turbulence shear stress: $\left\langle \overline{T_{xy}} \right\rangle_d \approx -\rho \left\langle \overline{u'\,v'} \right\rangle_d$. In this study, by following footprints of the effective eddy viscosity model of van Prooijen et al. (2005) and the concept of eddy viscosity model inside the cylinder arrays given by Kean and Smith (2013), a new hybrid eddy viscosity model to estimate $\left\langle \overline{T_{xy}} \right\rangle_d$ is proposed and validated using different experimental data sets.

The eddy viscosity model that was proposed for a compound channel without vegetation is used as a starting point. According to van Prooijen et al. (2005), the eddy viscosity is the contribution of two separate components, the eddy viscosity related to the bottom turbulence (υ_t') and the eddy viscosity associated with the LHCSs (υ_t'') and $\upsilon_t = \upsilon_t' + \upsilon_t''$. Both contributions are modeled as the product of a typical length and velocity scale LU related to their underlying mechanisms. The Elder formulation is adopted for the contribution by the bottom turbulence part (van Prooijen et al., 2005):

$$\upsilon_t' = \alpha\, D\, \sqrt{c_f}\, \left\langle \overline{u} \right\rangle_d \tag{8}$$

where α is a constant of the order of 0.1 (Fischer et al., 1979). The Prandtl's mixing length model is used to model the contribution of LHCSs to the total momentum exchange. Moreover, an extra factor which depends on the local water depth is incorporated in the model for the eddy viscosity related to the LHCSs (van Prooijen et al., 2005). The expression of the eddy viscosity linking to the LHCSs' part then reads

$$\upsilon_t'' = \frac{Dm}{D(y)}\, \beta^2\, \delta^2 \left| \frac{\mathrm{d}\left\langle \overline{u} \right\rangle_d}{\mathrm{d}y} \right| \tag{9}$$

In which β is a proportionality constant and δ is the mixing length. $D(y)$ is local water depth; D_m is the mean water depth; $D_m = \frac{D_c + D_f}{2}$; D_c is water depth in the channel, D_f is water depth in the floodplain channel.

In nonvegetated floodplain channels, the role of water depth ratio ($D_r = D_f/D_c$) has been acknowledged as it is shown to be associated with an increased shear rate and the consequent appearance of the LHCSs (Nezu et al., 1999; Knight et al., 2007). In vegetated channels, as the presence of vegetation appears to control the velocity gradient and thus the appearance of the LHCSs, the role of the water depth ratio D_r has received much less attention. It is noted that LHCSs originally arise from the Kelvin-Helmholtz (K-H) instability caused by the velocity gradient in the flow field. The differences in water depth or the drag from vegetation are elements contributing to this. Furthermore, the water depth ratio (D_r) is directly related to the vertical compression of the LHCSs and thereby may have an influence on the spreading of the LHCSs. These effects

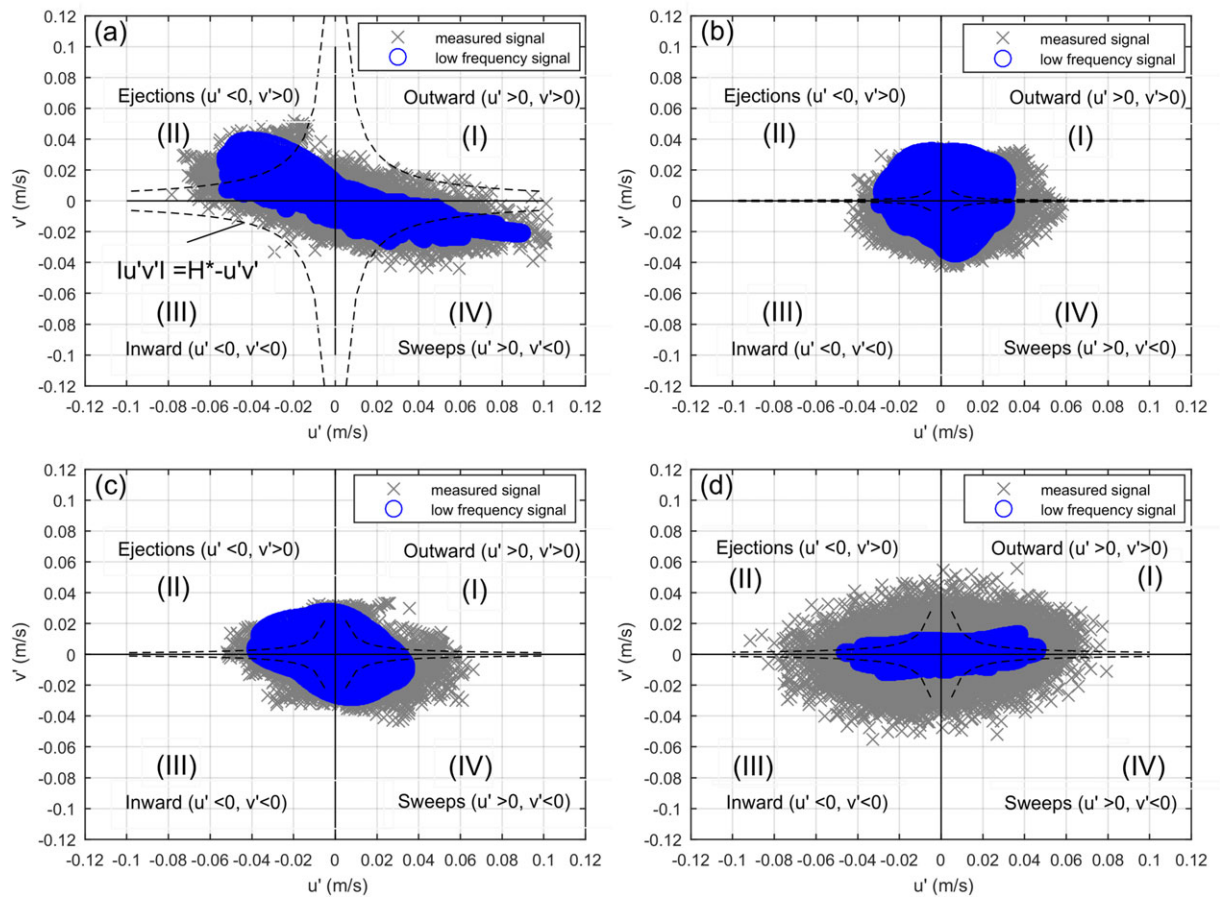

Figure 7. The representative distribution of (u', v') measured and the low-frequency signal for dense scenarios, q45h12: at location $y = 0$ m (at the vegetation interface), $H = 2$ (a); $y = -0.015$ m, $H = 2$ (b); $y = -0.065$ m (inside the vegetation), $H = 2$ (c); $y = 1.25$ m (in the main open channel), $H = 5$ (d); The dashed lines in the figure represent hyperbolas corresponding to $|u'\ v'| = H \cdot (-\overline{u'\ v'})$.

of the water depth ratio on the manifestation of the LHCSs can be accounted for by multiplying with D_r^2. The eddy viscosity associated with the manifestation of LHCSs then can be expressed as:

$$v_t'' = \frac{Dm}{D(y)} (D_r\ \beta)^2\ \delta^2 \left| \frac{\mathrm{d}\langle \overline{u} \rangle_d}{\mathrm{d}y} \right| \tag{10}$$

It is noted that v_t'' depends on the velocity gradient ($\mathrm{d}u/\mathrm{d}y$). In a single channel without floodplain and vegetation ($\mathrm{d}u/\mathrm{d}y = 0$), the LHCSs cannot be generated and thereby $v_t'' = 0$. Finally, the total eddy viscosity in nonvegetated compound channels can be written as:

$$v_t = \alpha \sqrt{c_f}\ \langle \overline{u} \rangle_d\ D + \frac{Dm}{D(y)}\ {D_r}^2\ \beta^2\ \delta^2 \left| \frac{\mathrm{d}\langle \overline{u} \rangle_d}{\mathrm{d}y} \right| \tag{11}$$

In studied scenarios, that is, compound channel, compound vegetated channel, and partially vegetated channel, the K-H instabilities are triggered primarily in the velocity gradient due to the water depth difference between the floodplain and adjacent channel region or the presence of the vegetation. The bottom friction only limits the growth of the mixing layer. Therefore, the interaction between the two terms in equation (11) is neglected and they can be considered independent.

In the literature, the mixing layer width can be estimated from the experimental data as the velocity difference between the main channel and the floodplain divided by the velocity gradient at the center of the velocity profile (Uijttewaal & Booij, 2000): $\delta = \frac{U_c - U_f}{(\partial U/\partial y)_{\max}}$. In order to take into account the asymmetry in the velocity profile, the mixing layer width is determined from the distance between position $y_{90\%}$ and $y_{10\%}$

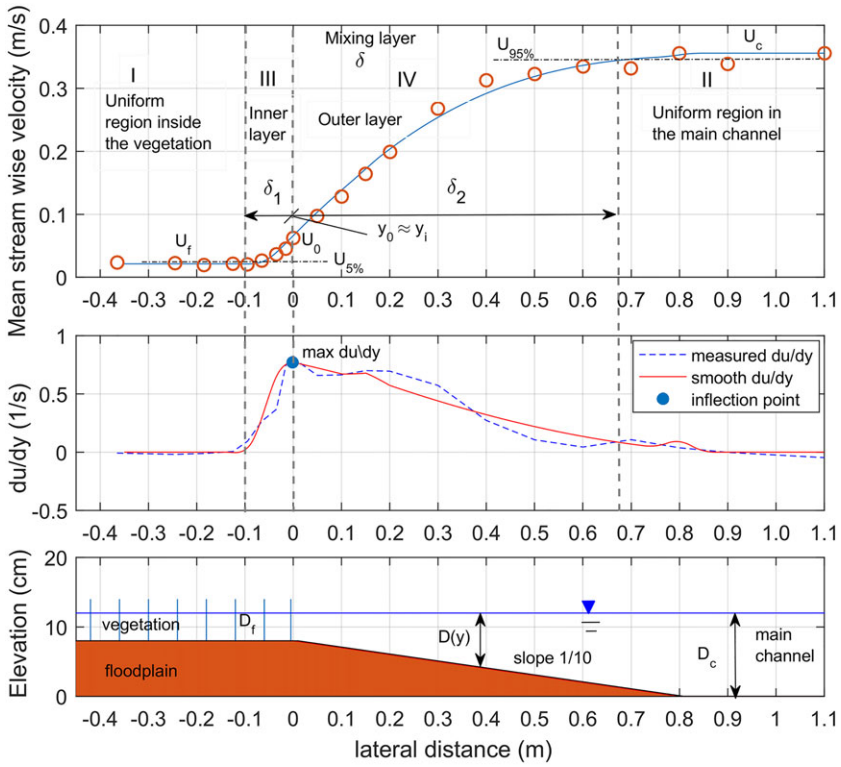

Figure 8. Representative mean streamwise velocity profile in cases with the consideration of vegetation. The most interesting region is the mixing layer, including the penetration (δ_1) or inner layer part and the outer layer part (δ_2). $Q = 45$ L/s, $H = 12$ cm, width = 50 cm.

(Pope, 2000): $\delta = y_{90\%} - y_{10\%}$, or position $y_{25\%}$ and $y_{75\%}$ (van Prooijen et al., 2005): $\delta = 2 \cdot \left(y_{75\%} - y_{25\%}\right)$ such that $U(y_{x\%}) = U_f + x\% \cdot (U_c - U_f)$.

However, these ways of determining the mixing layer width still do not well capture the asymmetrical feature of the mean streamwise velocity profile as there is usually a sharp decrease in the flow velocity near the vegetation edge (White & Nepf, 2007). Moreover, the penetration of the mixing layer into the vegetation region is not determined. Therefore, separating the mixing layer into two layers appears to be a better approach. In this way, the mixing layer width includes the penetration length scale of the mixing layer into the vegetation and the outer layer width can be calculated according to: $\delta_I \approx \max(0.5 \cdot (Cda)^{-1}, 1.8 \cdot d)$ and $\delta_o = \frac{U_c - U_m}{(dU/dy)_{ym}}$, where y_m is the matching point and $U_m = U(y_m)$ (White & Nepf, 2008). Still, the determination of the mixing layer width in this way is not likely to be consistent, and it is also unclear to what extent the accuracy of the penetration was considered.

In compound vegetated channels, the mean streamwise velocity profiles are also asymmetrical. At the edge of the vegetated floodplain, there is a sharp decrease corresponding to an inflection point in the velocity profile, which implies the effect of the shallower floodplain area and the presence of vegetation. Therefore, the mixing layer is divided into two layers, corresponding to the penetration layer and the outer layer: $\delta = \delta_1 + \delta_2$ (Figure 8). The penetration width of the mixing layer into the vegetation is defined as the distance required for the flow velocity to achieve a constant value inside the floodplain (U_f) plus an error of 5%. In other words, the penetration is the distance from the position where the mean streamwise velocity is 5% different from the uniform mean streamwise velocity further inside the floodplain (U_f) to the vegetated floodplain edge: $\delta_1 = y_0 - y_{5\%}$ and $U_{5\%} = U_f + 5\% \cdot U_f$. A similar rule is also applied for the outer layer width: $\delta_2 = y_{95\%} - y_0$ and $U_{95\%} = U_c - 5\%U_c$. This definition of the mixing layer width is consistent and allows determining the penetration precisely without any ambiguity. A typical streamwise velocity distribution is shown in Figure 8. The location y_0 is the point at the edge of the vegetated floodplain ($y = 0$ m). The point where the velocity gradient dU/dy reach its maximum value is the inflection point y_i. As y_i and y_0 are almost the same in all cases in the presence of vegetation, it can be considered that $y_i \approx y_0$.

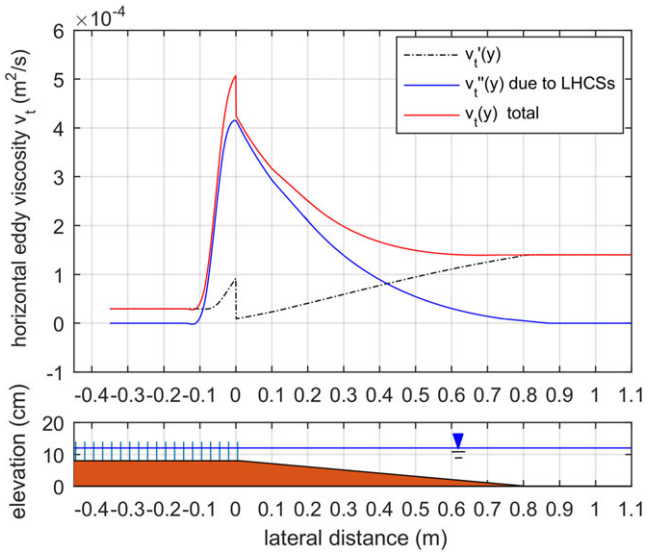

Figure 9. Eddy viscosity profile determined according to the hybrid eddy viscosity model and based on the measured velocity profile, in case of dense cylinder, $Q = 45$ L/s; $H = 12$ cm, and floodplain width $W = 50$ m.

The presence of vegetation can be taken into account by following the work of Kean and Smith (2013). Inside the vegetation, the eddy viscosity associated with the presence of vegetation (υ_{tv}) is determined from the production of turbulent kinetic energy by the flow through the stems and can be determined as

$$\upsilon_{\mathrm{tv}} = \frac{1}{8}\, C_t^{-2}\, C_d\, d\, \langle \overline{u} \rangle_d, \tag{12}$$

where C_t is a constant of proportionality, the value of it depends on the shape of the streamwise velocity profile, usually $C_t = 1$; C_d is the drag coefficient of a single stem, theoretically, $C_d = 1$. In this way, the eddy viscosity within the vegetation region including the part due to bottom friction, can be determined as

$$\upsilon_t' = \alpha\, \sqrt{c_f}\, \langle \overline{u} \rangle_d\, D + \frac{1}{8}\, C_t^{-2}\, C_d\, d\, \langle \overline{u} \rangle_d \tag{13}$$

Finally, with the presence of vegetation and LHCSs the total eddy viscosity can be calculated according to equation (14). It is also noticed that in cases without vegetation, equation (14) becomes equation (11). Figure 9 illustrates the eddy viscosity determined theoretically from equation (14) in cases of dense vegetation, floodplain width $H = 50$ cm, discharge $Q = 45$ L/s, and water level $H = 12$ cm.

$$\upsilon_t = \begin{cases} \alpha\, \sqrt{c_f}\, \langle \overline{u} \rangle_d\, D + \frac{Dm}{D(y)}\, D_r^{\,2}\, \beta^2\, \delta^2 \left| \frac{\mathrm{d}\langle \overline{u} \rangle_d}{\mathrm{d}y} \right| & \text{(outside vegetation)} \\ \underbrace{\alpha\, \sqrt{c_f}\, \langle \overline{u} \rangle_d\, D}_{\text{Elder}} + \underbrace{\frac{1}{8}\, C_t^{-2}\, C_d\, d\, \langle \overline{u} \rangle_d}_{\text{vegetation drag}} + \underbrace{\frac{D_m}{D(y)}\, D_r^{\,2}\, \beta^2\, \delta^2 \left| \frac{\mathrm{d}\langle \overline{u} \rangle_d}{\mathrm{d}y} \right|}_{\text{LHCSs}} & \text{(inside vegetation)} \end{cases} \tag{14}$$

9. Comparison With the Experimental Data

In this section, the hybrid eddy viscosity model is validated using different experimental data sets, including the current experiment of compound channels with and without vegetation, three representative experimental cases of White and Nepf (2007) in partially vegetated channels and the experimental results of Lambert and Sellin (1996) and Ervine et al. (2000) in compound channels without vegetation. Additionally, the transverse shear stresses determined from the hybrid eddy viscosity model was compared with that calculated from the eddy viscosity models of White and Nepf (2008) and van Prooijen et al. (2005). The results show the applicability of the hybrid eddy viscosity model.

To begin with, as the measured and collected data include the RSs ($-\left\langle \overline{u'\, v'} \right\rangle_d$), the measured momentum transfer is determined by

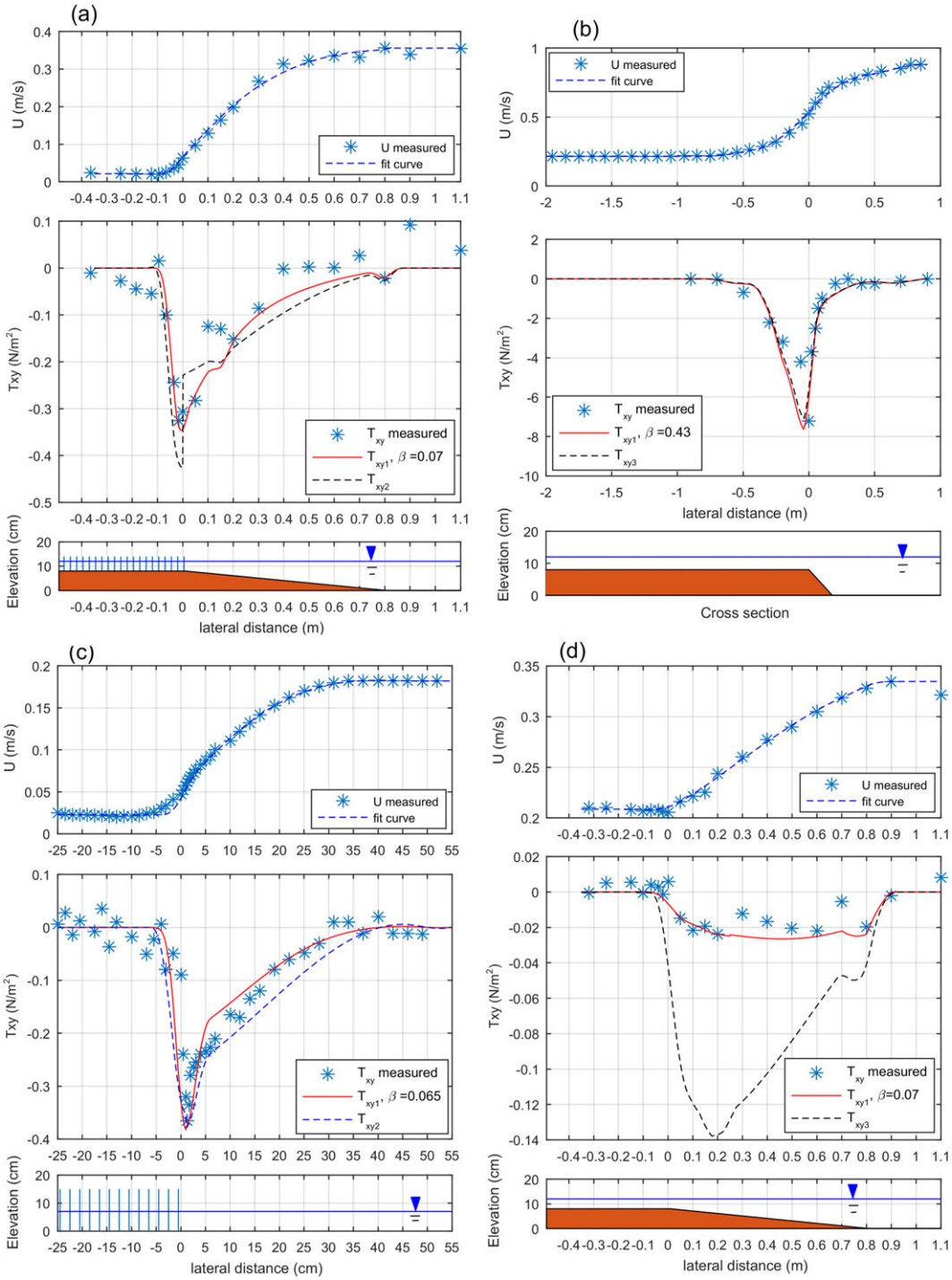

Figure 10. Comparison of transverse momentum exchange between the measurement data (T_{xy}measured), eddy viscosity model of White and Nepf (2008; T_{xy2}), the new hybrid eddy viscosity model (T_{xy1}), and the effective eddy viscosity of van Prooijen et al., (2005; T_{xy3}) in the current experiment, case Ad1 and An1: dense and no vegetation, $Q = 45$ L/s; $H = 12$ cm, and floodplain width $W = 50$ m (left upper panel and right lower panel, respectively); in the experiment of Lambert and Sellin (1996; right upper panel); and in the experiment of White and Nepf (2007), case I (left lower panel).

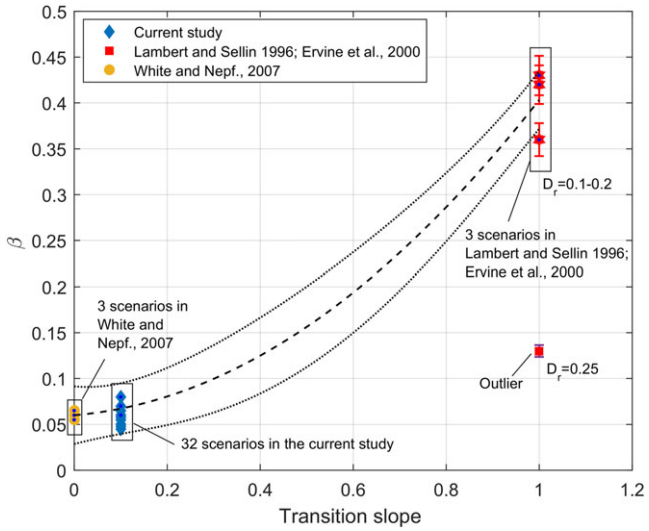

Figure 11. A possible relationship between the beta and the transition slope based on the three representative scenarios from White and Nepf (2007), 32 scenarios from the current study and 3 scenarios from Lambert and Sellin (1996) and Ervine et al. (2000) (in total 38 scenarios), dashed line: fitted curve; dotted line: prediction bound.

$$T_{xy\text{measure}} = -\rho \left\langle \overline{u'\, v'} \right\rangle_d \tag{15}$$

Furthermore, as described in the previous sections, the theoretical eddy viscosity model (υ_t) was determined from equation (14). In all scenarios, the depth average mean streamwise velocity profiles along the cross section of the flume were plotted. Within the vegetation area, the velocity was spatially averaged to remove cylinder-scale spatial fluctuations in the arrays. A fourth-order polynomial line was drawn through the measurement points. Then, following the definitions in the previous section, the velocity gradient, the inner layer width, outer layer width, and the width of the mixing layer were determined. Finally, the transverse shear stresses based on the hybrid eddy viscosity model (T_{xy1}) were determined using

$$T_{xy1} = -\rho\, \upsilon_t \frac{\partial U}{\partial y} \tag{16}$$

Moreover, the transverse shear stresses were also determined from the vortex-based model of White and Nepf (2008) (T_{xy2}) in scenarios with vegetation, and from the effective eddy viscosity concept of van Prooijen et al. (2005) for cases of compound channel flows without vegetation (T_{xy3}; definitions in Table 1). Figure 10 illustrates the validation and comparison of the transverse momentum exchange determined from the different eddy viscosity models. Representative results for different scenarios are presented in the Appendix (Figures A2 to A6). The complete set is presented in the supporting information of this paper.

In cases of compound vegetated channels, the model of White and Nepf (2008) produces a relatively good result of the transverse momentum exchange. However, it is likely to overestimate the peak of the lateral momentum transfer, the momentum transfer inside the vegetation, and the momentum transfer in the outer layer. In cases of compound channels, the model of van Prooijen et al. (2005) significantly overestimates the lateral momentum exchange.

It is suggested that by changing only the values of the proportional coefficient (β) with an average value of 0.0625 for mild slopes, the depth-averaged transverse momentum exchange determined from the hybrid eddy viscosity model can fit different experimental data sets, including the 32 scenarios of the current experiment and three representative scenarios of partially vegetated channels. In the scenarios of unvegetated compound channels of Lambert and Sellin (1996) and Ervine et al. (2000), the β values increased to about 0.42. The difference in the transition slope is likely to be the main reason for the increase of the β value. A possible relationship between the β value and the transition slope can be seen in Figure 11, with only one scenario of a compound channel without vegetation (slope 1:1, $D_r = 0.25$), in which the value of β significantly drops to about 0.13. It is noticed that for a steep slope, as the water depth increases, the contribution of secondary circulations to the momentum exchange increases and becomes dominant over the contribution of the turbulent mixing (Tominaga & Nezu, 1991; Vermaas et al., 2011). Therefore, this outlier of the β value is likely due to the effect of the secondary flow triggered by the increased water depth, which was not included in the current hybrid model.

10. Conclusions

In a vegetated compound channel, the transverse exchange of mass and momentum between the open main channel and the region of vegetation governs the sediment and nutrient transport, which has lots of ecological implications. The presence of the LHCSs and their associated cycloid flow events are the major factors contributing to this momentum exchange. However, the understanding of this phenomenon is still incomplete. As a result, the momentum exchange models developed in previous studies appear to be not applicable for different scenarios as their validity is usually restricted to a particular experiment data set.

In this study, with the purpose of getting insight into the transverse momentum exchange, a unique experiment has been conducted. Based on the results of the experiment, a quadrant analysis of the RSs has been performed. The results revealed the connection between the LHCSs, their associated flow events, and the

transverse momentum exchange. Moreover, the appearances of the cycloid flow events as well as the way in which different locations in the flow field are affected by the LHCSs were analyzed. The most up-to-date momentum exchange models were reviewed and verified with the data from the experiment. A new hybrid eddy viscosity model is proposed and validated using different experiment data sets. The results suggested that by varying only a coefficient of proportionality β related to the forcing of the mixing layer, which significantly depends on the transition slope, the transverse momentum exchange can be well modeled for quite a range of different setups and scenarios of compound channels with or without vegetation. Limitations are still found for steep slope cases where secondary circulation can play a significant role in the momentum transport.

Now the generic applicability of the viscosity estimation has been demonstrated, it can be used as a turbulent model representing the large-scale structures in numerical simulations of compound channel flow. The numerical model can be run first with traditional eddy viscosity model such as Elder formulation. Based on the simulation results, the presence of LHCSs can be checked, and the shear-layer width can be determined. This value can be used to iteratively calculate the eddy viscosity according to the hybrid eddy viscosity model and imposed again into the constructed model to improve the results in terms of velocity and especially the Reynold shear stress.

Appendix A

A1. Experimental Conditions

The mean streamwise velocity was measured using a Nortek Acoustic Doppler Velocity meter (ADV) at a sampling rate of 25 Hz. Velocity measurements were taken over a time interval of 10 min. Moreover, in order to improve the quality of the ADV signal, an electrolyzer with 0.1-mm-thick wires was placed about 15 cm ahead from the ADV. In the experiments, the correlations are larger than 85–95%, and the dimensionless signal-to-noise ratios (SNR) exceed 18 dB in all measurement scenarios.

The movement of flow were measured by Particle Image Velocimetry (PIV). Floating black polypropylene tracer particles with a diameter of around 2 mm were used. A RedLake 1 MegaPixel digital camera with a resolution of 1008 × 1018 pixels has been used to capture frames and was installed on the top of a frame build on a movable platform constructed over the flume. The measurement duration was 300 s. The average particle displacement has been computed to acquire the instantaneous surface velocity fields.

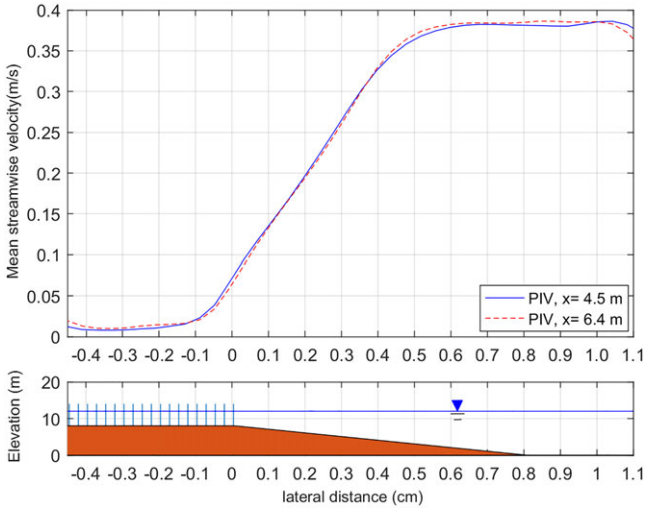

Figure A1. Representative streamwise velocity at different locations along the flume ($x = 4.5$ m and $x = 6.4$ m) determined from the PIV measurement. It is suggested that a fully developed flow field can be safely achieved at location $x = 5$ m.

Table A1
Experiment Configurations and Major Results

Cases	An1	An2	An3	An4	Bn1	Bn2	Bn3	Bn4	As1	As2	As3	As4	Bs1	Bs2	Bs3	Bs4
N (number/m^2)	0	0	0	0	0	0	0	0	139	139	139	139	139	139	139	139
Φ	0	0	0	0	0	0	0	0	0	0	0	0	0.01	0.01	0.01	0.01
$C_D \cdot a$	0	0	0	0	0	0	0	0	0.029	0.025	0.028	0.027	0.019	0.019	0.017	0.019
Width (m)	50	50	50	50	25	25	25	25	50	50	50	50	25	25	25	25
$Q(L^{-1})$	45	60	80	80	45	60	80	80	45	60	80	80	45	60	80	80
D_f (cm)	3.9	4.84	6.26	4.4	4.13	5.12	6.47	4.11	4.76	5.17	6.47	4.59	4.82	5.59	6.28	4.66
D_c (cm)	11.9	12.84	14.26	12.4	12.13	13.12	14.47	12.11	12.76	13.17	14.47	12.59	12.82	13.59	14.28	12.66
$Dr = D_f/D_c$	0.33	0.38	0.44	0.35	0.34	0.39	0.45	0.34	0.37	0.39	0.45	0.36	0.38	0.41	0.44	0.37
Fr	0.33	0.41	0.44	0.58	0.32	0.38	0.41	0.59	0.29	0.36	0.4	0.5	0.27	0.32	0.39	0.47
$R_ec(\times 10^3)$	39.83	49.55	61.57	62.05	39.93	51.23	65.3	64.87	41.03	53.53	69.09	69.49	38.87	49.79	66	65.95
$R_ef(\times 10^3)$	8.02	13.64	21.81	16.7	8.32	13.62	21.38	15.29	2.27	3.57	4.86	4.63	2.3	3.35	4.6	4.28
U_f(cm s)	20.9	28.2	34.9	38	20.2	26.6	33.2	37.3	4.8	6.9	7.9	9.8	4	5.3	6.3	8.4
U_c(cm s)	33.5	39.8	44.4	51.5	34.9	41.3	47.4	56.3	33.3	42.1	49.6	56.9	33.2	40.3	50.3	56.5
U_o(cm s)	20.9	28.2	34.9	38	22.5	29.6	35.8	41.3	8.7	11.3	13	15.5	9.4	12.3	15.5	18
U_s(cm s)	0	0	0	0	2.4	3	2.6	4.1	3.9	4.4	5.1	5.7	5.4	7	9.3	9.7
u_*	0.2	0.5	0.5	0.7	0.3	0.5	0.8	0.7	3.9	5.1	8.2	10.4	5.5	7.9	13	16.2
y_i (cm)	72	89	89.8	83.9	50	50	50	50	50	50	50	50	50	50	50	50
δ_1	0	0	0	0	6.6	6.6	4	5.4	9.8	8.8	8.9	8.1	9.2	9.2	9.3	8.9
δ_2(cm)	47.5	28.7	22.5	31	66.3	58.6	51.2	61.6	57.5	56.7	54.2	56.8	60.9	57.2	52.4	54
δ (cm)	69.5	67.7	62.3	64.9	72.9	65.2	55.2	67	67.3	65.5	63.1	64.9	70.1	66.4	61.7	62.9
β	0.07	0.065	0.07	0.07	0.065	0.065	0.07	0.07	0.08	0.08	0.08	0.08	0.065	0.065	0.065	0.065

Cases	Cs1	Cs2	Cs3	Cs4	Ad1	Ad2	Ad3	Ad4	Bd1	Bd2	Bd3	Bd4	Cd1	Cd2	Cd3	Cd4
N (number/m^2)	139	139	139	139	556	556	556	556	556	556	556	556	556	556	556	556
Φ	0.01	0.01	0.01	0.01	0.04	0.04	0.04	0.04	0.04	0.04	0.04	0.04	0.04	0.04	0.04	0.04
$C_D \cdot a$	0.019	0.013	0.012	0.012	0.094	0.153	0.132	0.106	0.124	0.115	0.127	0.089	0.117	0.084	0.054	0.059
Width (m)	10	10	10	10	50	50	50	50	25	25	25	25	10	10	10	10
$Q(L^{-1})$	45	60	80	80	45	60	80	80	45	60	80	80	45	60	80	80
D_f (cm)	4.4	5.11	6.49	4.44	4.22	5.21	6.42	4.64	4.33	5.43	6.74	4.53	4.47	5.75	6.49	4.47
D_c (cm)	12.4	13.11	14.49	12.44	12.22	13.21	14.42	12.64	12.33	13.43	14.74	12.53	12.47	13.75	14.49	12.47
$Dr = D_f/D_c$	0.35	0.39	0.45	0.36	0.35	0.39	0.44	0.37	0.35	0.4	0.46	0.36	0.36	0.42	0.45	0.36
Fr	0.26	0.32	0.35	0.45	0.31	0.36	0.42	0.52	0.29	0.33	0.36	0.47	0.31	0.34	0.41	0.51
$R_ec(\times 10^3)$	34.92	47.36	61.23	62.3	41.4	53.7	71.48	72.83	39.42	51.3	64.41	64.98	42.37	53.75	70.1	71.03
$R_ef(\times 10^3)$	2.83	4.38	6.69	5.59	0.9	1.03	1.39	1.7	0.95	1.42	1.79	2.01	1.83	3.02	4.62	3.44
U_f(cm s)	3.5	2.6	7.2	8.9	2.1	2.1	2.2	3.7	2.2	2.6	2.7	4.5	1	1	1.6	2.5
U_c(cm s)	34.2	42.5	49.6	58.4	35.6	41.9	51.5	58.7	34.9	41.2	48.3	58.5	35	40.2	50	59.3
U_o(cm s)	11.7	13.2	16.6	19.7	6.6	7.8	8.6	11.1	8.9	11.7	14.3	16.4	8.9	12	15.8	17.1
U_s(cm s)	8.2	10.6	9.4	10.8	4.5	5.8	6.4	7.5	6.7	9	11.7	11.9	7.9	11	14.2	14.6
u_*	3.1	5.8	9.4	11	3.3	5.8	8.5	8.5	5.1	9.3	13.2	16.27	4.8	8.2	14.8	15.8
y_i (cm)	50	50	50	50	50	50	50	50	50	50	50	50	50	50	50	50
δ_1	10	10	10	10	7.6	8.4	8.7	7	8.3	8.1	8.4	6.8	10	10	10	10
δ_2 (cm)	51.4	41.7	38	40.6	61.3	64	62.8	59.7	60.1	56.5	54.4	59.3	48.5	45.9	43.2	47.7
δ (cm)	61.4	51.7	48	50.6	68.9	72.4	71.5	66.7	68.4	64.6	62.8	66.1	58.5	55.9	53.2	57.7
β	0.045	0.045	0.048	0.045	0.07	0.065	0.06	0.07	0.058	0.06	0.055	0.055	0.048	0.05	0.045	0.055

A2. Hybrid Eddy Viscosity Model Validation

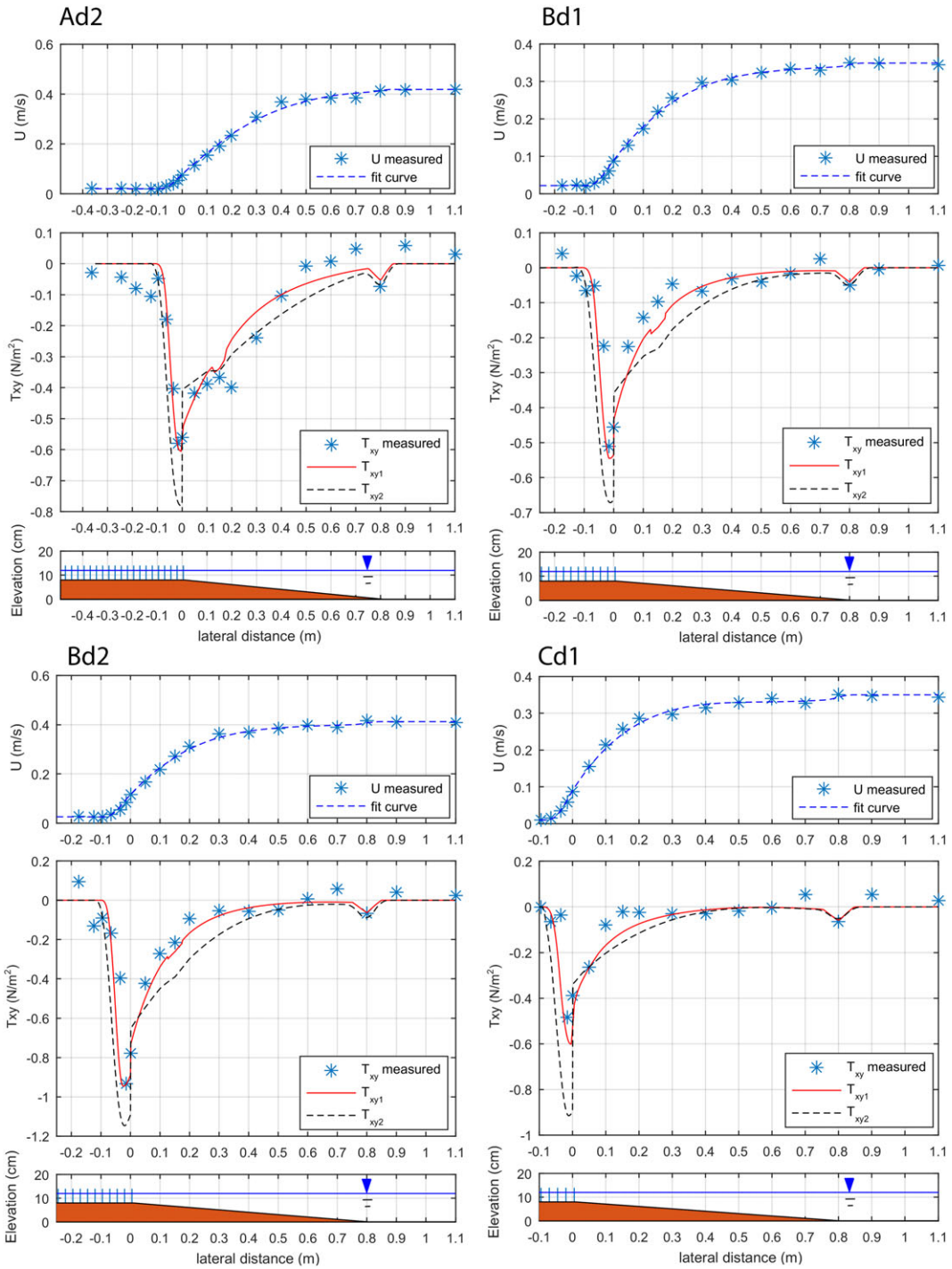

Figure A2. Profile of mean streamwise velocity and the comparison of modeled transverse shear stress according to the eddy viscosity model of this study T_{xy1}, in cases Ad2, Bd1, Bd2, and Cd1 (left upper panel, right upper panel, left lower panel, and right lower panel, respectively), and T_{xy2} (White & Nepf, 2008).

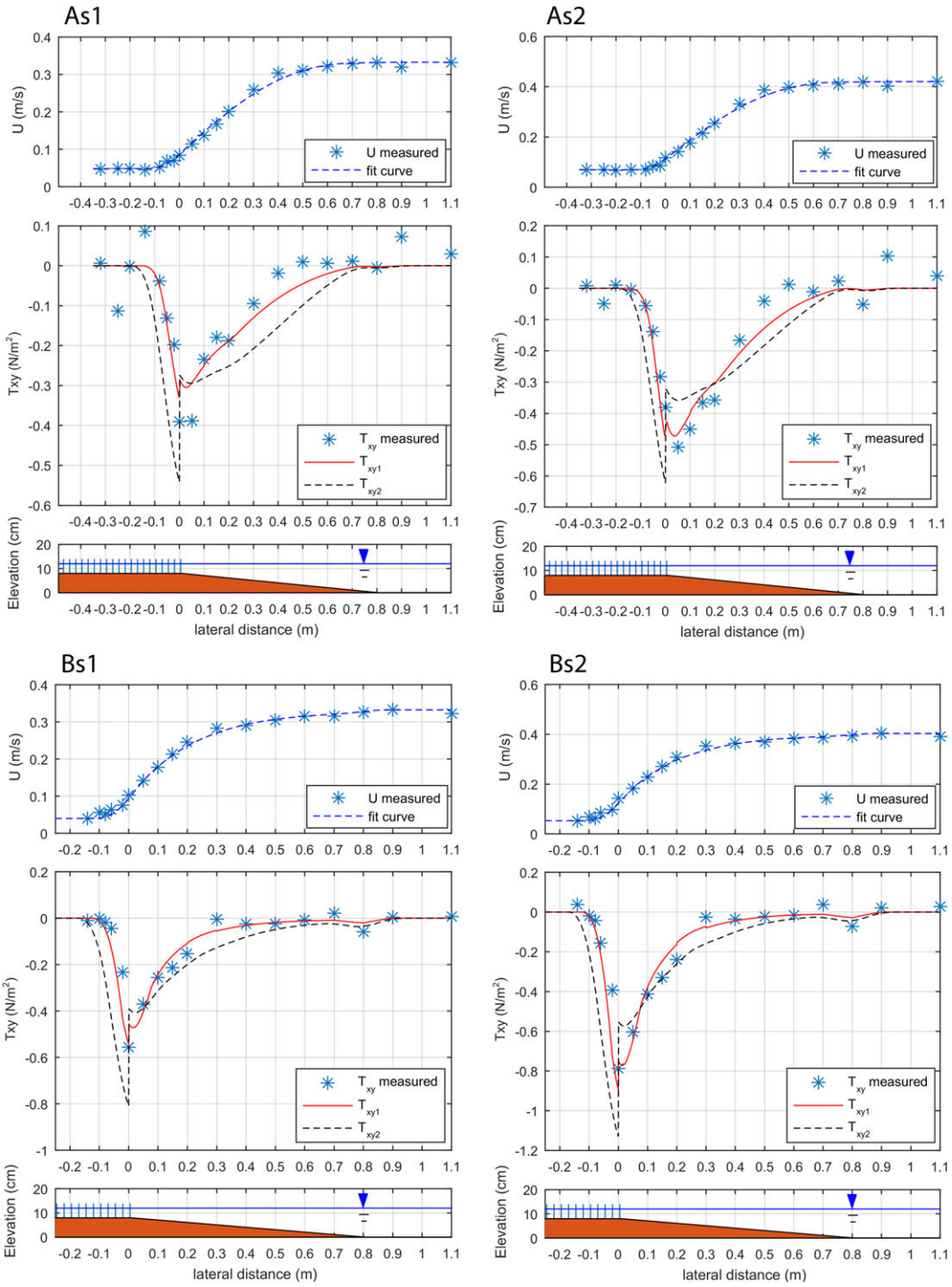

Figure A3. Profile of mean streamwise velocity and the comparison of modeled transverse shear stress according to the eddy viscosity model of this study T_{xy1}, in cases As1, As2, Bs1, and Bs2 (left upper panel, right upper panel, left lower panel, and right lower panel, respectively), and T_{xy2} (White & Nepf, 2008).

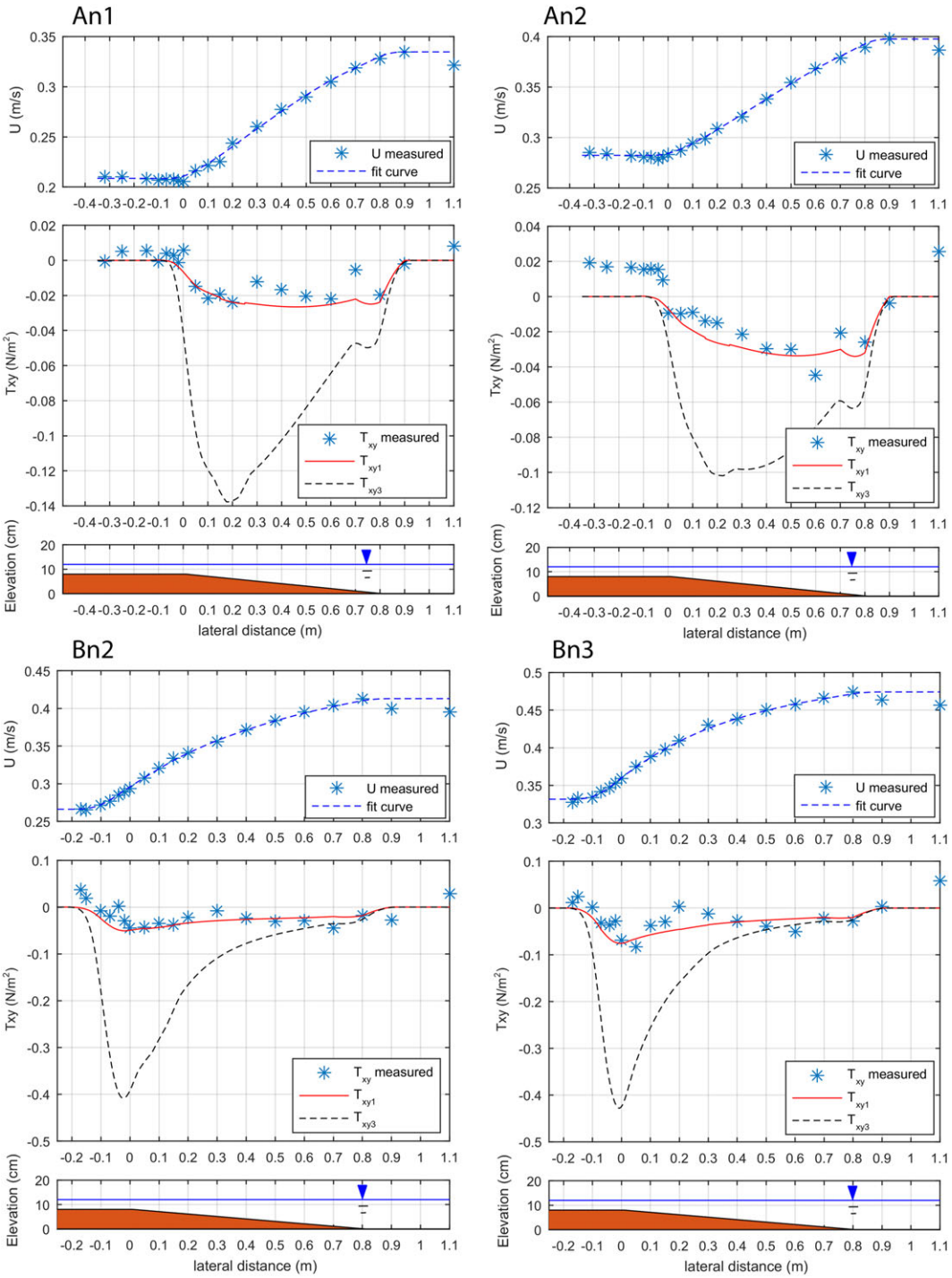

Figure A4. Profile of mean streamwise velocity and the comparison of modeled transverse shear stress according to the eddy viscosity model of this study T_{xy1}, in cases An1, An2, Bn2, and Bn3 (left upper panel, right upper panel, left lower panel, and right lower panel, respectively), and T_{xy3} (van Prooijen et al., 2005).

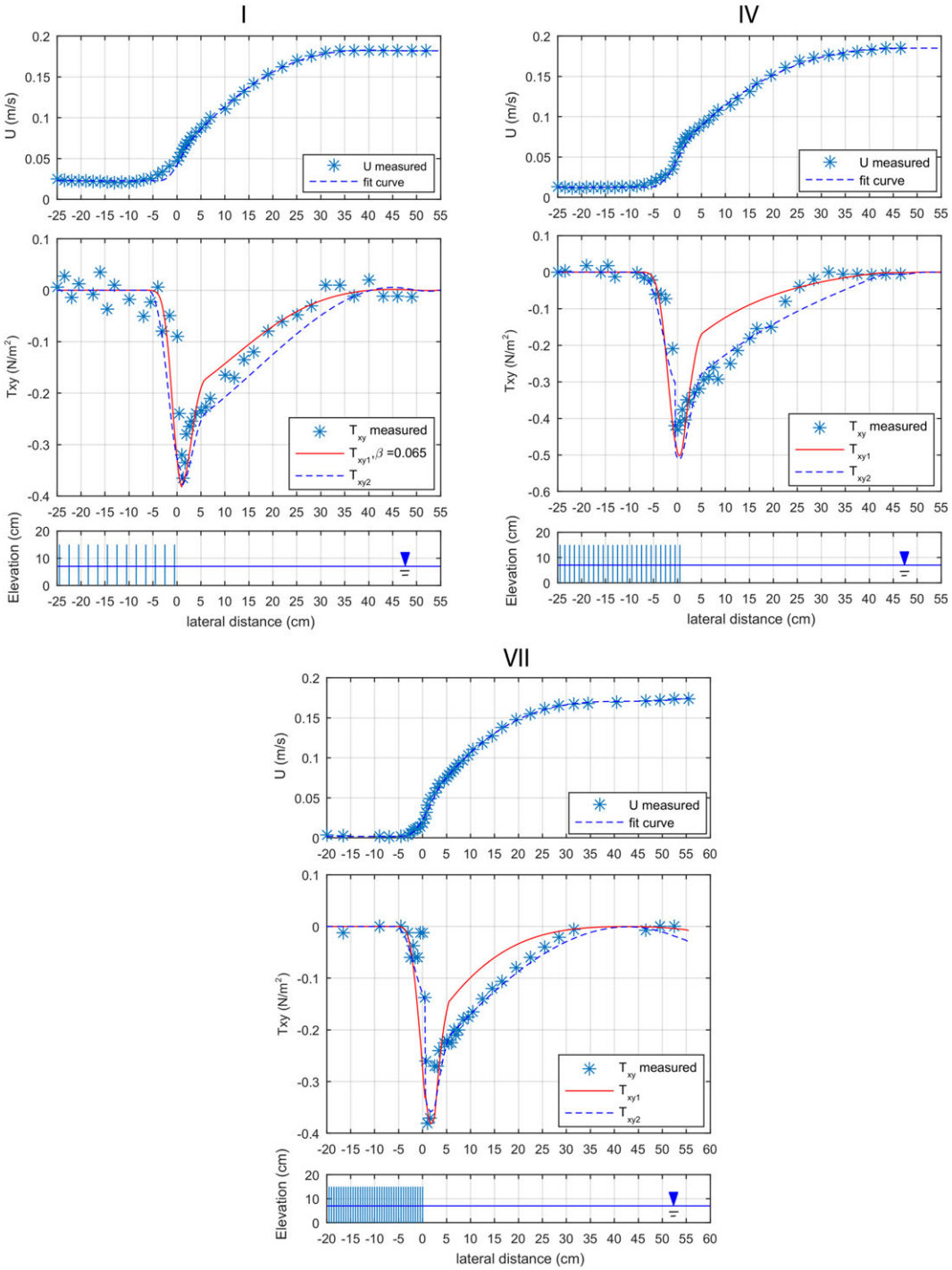

Figure A5. Profile of mean streamwise velocity and the comparison of modeled transverse shear stress according to the eddy viscosity model of this study T_{xy1}, in cases I, IV, and VII of White and Nepf (2007; left upper panel, right upper panel, lower panel, respectively), and T_{xy2} (White & Nepf, 2008).

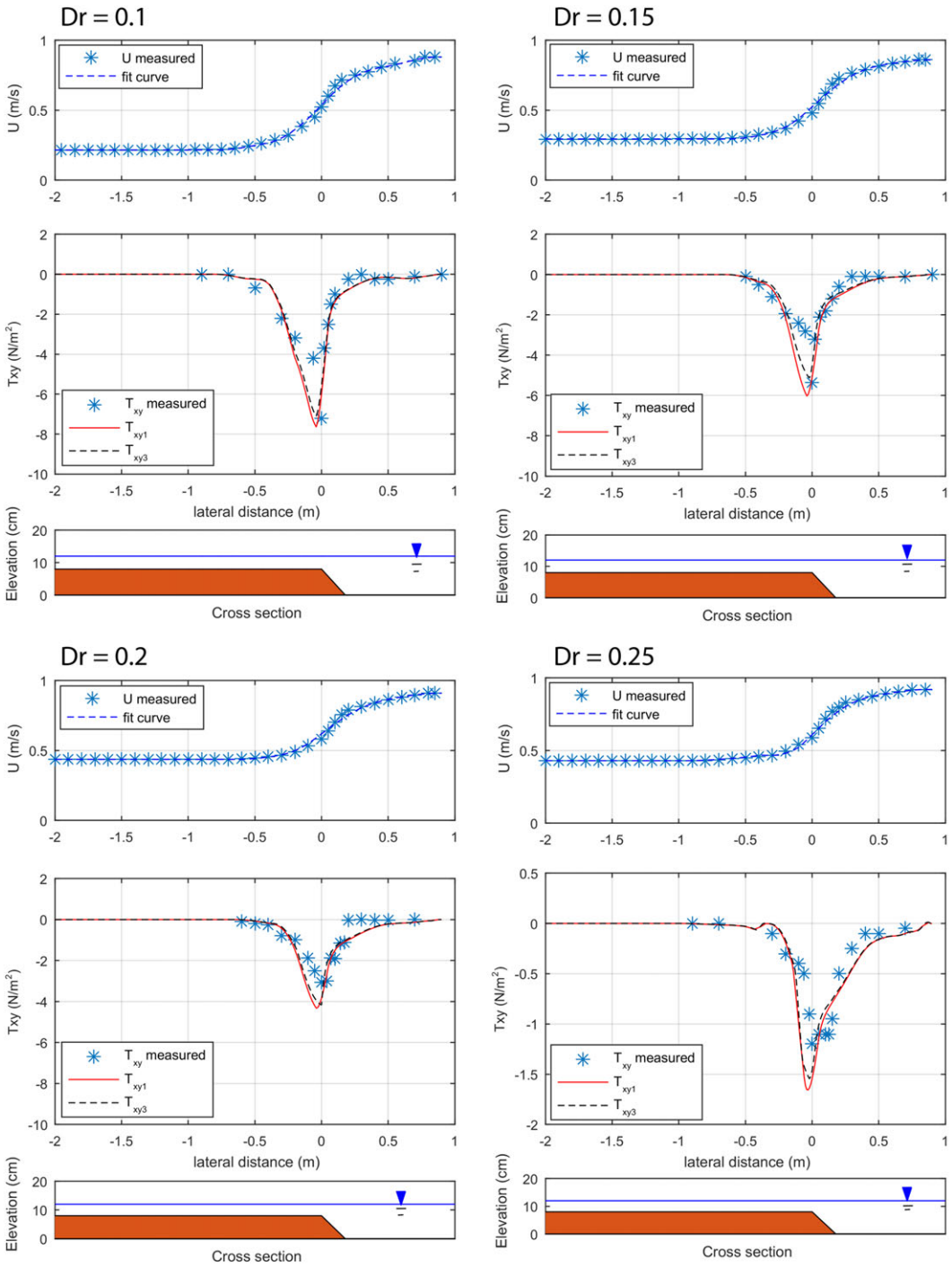

Figure A6. Profile of mean streamwise velocity and the comparison of modeled transverse shear stress according to the eddy viscosity model of this study T_{xy1}, in cases $D_r = 0.11$, 0.15, 0.20, and 0.25 of Lambert and Sellin (1996) and Ervine et al. (2000; left upper panel, right upper panel, left lower panel and right lower panel, respectively), and T_{xy3} (van Prooijen et al., 2005).

A3. List of Symbols

a	Average solid frontal area per unit volume in the plane perpendicular to the flow (m^{-1})
β	constant (-)
C_f	Bed friction coefficient (-)
C_d	Drag coefficient of the array element (-)
Cda	Vegetation drag (m^{-1})
C_t	A constant of proportionality (-)
d	Cylinder diameter (m)
$D(y)$	Local water depth (m)
D_c	Water depth in the main channel (m)
D_f	Water depth in the floodplain channel (m)
D_m	Mean water depth (m)
D_r	Water depth ratio (-)
$\mathrm{d}u/\mathrm{d}y$	Velocity gradient (s^{-1})
D_x	Drag force exerted on the fluid in the x-direction (N)
F_r	Froude number (-)
f_{filter}	Filter frequency (Hz)
H	Water level (m)
N	Density of cylinders (number/m^2)
n	Porosity (-)
ζ	Water level above and arbitrary horizontal reference plane (m)
ρ	Mass density (kg/m^3)
Q	Discharge (L/s)
Re_c	Reynolds number in the main channel (-)
Re_f	Reynolds number in the floodplain channel (-)
s	Distance between cylinders (m)
δ_1	Inner layer width (m)
δ_2	Outer layer width (m)
$\left\langle \overline{T_{xy}} \right\rangle_d$	Time- and depth-averaged transverse shear stress (N/m^2)
$T_{xy\mathrm{measure}}$	Measured momentum transfer (N/m^2)
T_{xy1}	Transverse shear stresses based on the hybrud eddy viscosity model (N/m^2)
T_{xy2}	Transverse shear stresses determined from the vortex-based model (N/m^2)
T_{xy3}	Transverse shear stresses determined from effective eddy viscosity model (N/m^2)
U_c	Uniform mean streamwise velocity in the main channel (m/s)
U_f	Uniform mean streamwise velocity in the floodplain channel (m/s)
U_o	Mean streamwise velocity at y_o (m/s)
U_s	Interfacial slip velocity (m/s)
U_m	Mean streamwise velocity at the matching point (m/s)
$\left\langle \overline{u} \right\rangle_d, \left\langle \overline{v} \right\rangle_d$	Time-averaged, spatially averaged, and depth-averaged streamwise and transverse velocities (m/s)
u_*	Friction velocity (m/s)
u', v'	Streamwise and transverse velocity temporal fluctuation (m/s)
u'', v''	Streamwise and transverse velocity spatial fluctuation (m/s)
ν_t	Eddy viscosity (m^2/s)
ν_t'	Eddy viscosity related to the bottom turbulence (m^2/s)
ν_t''	Eddy viscosity associated with the LHCSs (m^2/s)
ν_{tv}	Eddy viscosity associated with the presence of vegetation (m^2/s)
δ	Mixing length (m)
W	Floodplain width (m)
y_i	Inflection point (m)
y_m	Matching point (m)
y_0	Point at the edge of vegetated floodplain (m)
Φ	Solid volume fraction (-)

Acknowledgments
This study is supported by the Ministry of Education and Training scholarship (MOET), Vietnam, the Delft University of Technology, the Netherlands, and the ThuyLoi University Hanoi, Vietnam. The data used are listed in the references, tables, figures, and supporting information.

References

Adrian, R. J., & Marusic, I. (2012). Coherent structures in flow over hydraulic engineering surfaces. *Journal of Hydraulic Research*, *50*(5), 451–464.
Bousmar, D. (2002). Flow modelling in compound channels (PhD thesis). Civil et Environnemental, Uniré de Génie.
Chen, D., & Jirka, G. H. (1997). Absolute and convective instabilities of plane turbulent wakes in a shallow water layer. *Journal of Fluid Mechanics*, *338*, 157–172.
Drazin, P. G., & Reid, W. H. (2004). *Hydrodynamic stability*. Chicago: University of Chicago.
Ervine, D. A., Babaeyan-Koopaei, K., & Sellin, R. H. J. (2000). Two-dimensional solution for straight and meandering overbank flows. *Journal of Hydraulic Engineering*, *126*(9), 653–669.
Fernandes, J. N., Leal, J. B., & Cardoso, A. H. (2014). Improvement of the lateral distribution method based on the mixing layer theory. *Advances in Water Resources*, *69*, 159–167.
Fischer, H. B., List, E. J., Koh, C. R., Imberrger, J., & Brooks, N. H. (1979). *Mixing in inland and coastal waters*. San Diego, CA: Academic Press. https://doi.org/10.1016/B978-0-08-051177-1.50020-9
Helmiö, T. (2004). Flow resistance due to lateral momentum transfer in partially vegetated rivers. *Water Resources Research*, *40*, W05206. https://doi.org/10.1029/2004WR003058
Ikeda, S., Izumi, N., & Ito, R. (1991). Effects of pile dikes on flow retardation and sediment transport. *Journal of Hydraulic Engineering-asce - J HYDRAUL ENG-ASCE*, *117*, 1459–1478.
Kean, J. W., & Smith, J. D. (2013). Flow and boundary shear stress in channels with woody bank vegetation. In S. J. Bennett & A. Simon (Eds.), *Riparian vegetation and fluvial geomorphology* (pp. 237–252). Washington, DC: American Geophysical Union. https://doi.org/10.1029/008WSA17
Kim, J., & Moin, P. (1986). The structure of the vorticity field in turbulent channel flow. Part 2. Study of ensemble-averaged fields. *Journal of Fluid Mechanics*, *162*, 339–363.
Kim, J., Moin, P., & Moser, R. (1987). Turbulence statistics in fully developed channel flow at low Reynolds number. *Journal of Fluid Mechanics*, *177*, 133–166.
Knight, D. W., Aya, S., Ikeda, S., Nezu, I., & Shiono, K. (2007). *Flow and sediment transport in compound channels, the experiences of Japanese and UK Research, chap. 2: Flow structure* (pp. 5–113). IAHR Monographs.
Lambert, M. F., & Sellin, R. H. J. (1996). Discharge prediction in straight compound channels using the mixing length concept. *Journal of Hydraulic Research*, *34*(3), 381–394.
Mazda, Y., Wolanski, E., King, B., Sase, A., Ohtsuka, D., & Magi, M. (1997). Drag force due to vegetation in mangrove swamps. *Mangroves and Salt Marshes*, *1*, 193–199. https://doi.org/10.1023/A:1009949411068
Nadaoka, K., & Yagi, H. (1998). Shallow-water turbulence modeling and horizontal large-eddy computation of river flow. *Journal of Hydraulic Engineering*, *124*(5), 493–500. https://doi.org/10.1061/(ASCE)0733-9429(1998)124:5(493)
Nepf, H. M. (1999). Drag, turbulence, and diffusion in flow through emergent vegetation. *Water Resources Research*, *35*(2), 479–489.
Nezu, I., & Onitsuka, K. (2001). Turbulent structures in partly vegetated open-channel flows with LDA and PI V measurements. *Journal of Hydraulic Research*, *39*(6), 629–642. https://doi.org/10.1080/00221686.2001.9628292
Nezu, I., Onitsuka, K., & Iketani, K. (1999). Coherent horizontal vortices in compound open-channel flows. In V. P. Singh, I. W. Seo, & J. H. Sonu (Eds.), *Hydraulic Modeling* (pp. 17–32). Seoul, Korea: Water Resources Publication.
Nezu, I., & Sanjou, M. (2008). Turburence structure and coherent motion in vegetated canopy open-channel flows. *Journal of Hdro-Environment Research*, *2*(2), 62–90.
Pasche, E., & Rouve, G. (1985). Overbank flow with vegetatively roughened flood plains. *Journal of Hydraulic Engineering*, *111*(9), 1262–1278. https://doi.org/10.1061/(ASCE)0733-9429(1985)111:9(1262)
Phan, L. K., van Thiel de Vries, J. S. M., & Stive, M. J. F. (2015). Coastal mangrove squeeze in the Mekong Delta. *Journal of Coastal Research*, *300*, 233–243. https://doi.org/10.2112/JCOASTRES-D-14-00049.1
Poggi, D., Katul, G. G., & Albertson, J. D. (2004). A note on the contribution of dispersive fluxes to momentum transfer within canopies. *Boundary-Layer Meteorology*, *111*(3), 615–621.
Poggi, D., Porporato, A., Ridolfi, L., Albertson, J. D., & Katul, G. G. (2004). The effect of vegetation density on canopy sub-layer turbulence. *Boundary-Layer Meteorology*, *111*(3), 565–587.
Pope, S. B. (2000). *Turbulent flows*. New York: Cambridge University Press.
Talstra, H. (2011). Large-scale turbulence structures in shallow separating flows (PhD thesis).
Tamai, N., Asaeda, T., & Ikeda, H. (1986). Study on generation of periodical large surface eddies in a composite channel flow. *Water Resources Research*, *22*(7), 1129–1138. https://doi.org/10.1029/WR022i007p01129
Tominaga, A., & Nezu, I. (1991). Turbulent structure in compound open-channel flows. *Journal of Hydraulic Engineering*, *177*(1), 21–41. https://doi.org/10.1061/(ASCE)0733-9429(1991)117:1(21)
Truong, S. H., Ye, Q., & Stive, M. J. F. (2017). Estuarine mangrove squeeze in the Mekong Delta, Vietnam. *Journal of Coastal Research*, *33*(4), 747–764. https://doi.org/10.2112/JCOASTRES-D-16-00087.1
Uijttewaal, W. S. J., & Booij, R. (2000). Effects of shallowness on the development of free-surface mixing layers. *Physics of Fluids*, *12*(2), 392–402.
van Prooijen, B. C. (2004). Shallow mixing layers (Ph.D thesis), Delft University of Technology The Netherlands.
van Prooijen, B. C., Battjes, J. A., & Uijttewaal, W. S. J. (2005). Momentum exchange in straight uniform compound channel flow. *Journal of Hydraulic Engineering*, *131*(3), 175–183. https://doi.org/10.1061/(ASCE)0733-9429(2005)131:3(175)
Vermaas, D. A., Uijttewaal, W. S. J., & Hoitink, A. J. F. (2011). Lateral transfer of streamwise momentum caused by a roughness transition across a shallow channel. *Water Resources Research*, *47*, W02530. https://doi.org/10.1029/2010WR010138
Vionnet, C. A., Tassi, P. A., & Martín Vide, J. P. (2004). Estimates of flow resistance and eddy viscosity coefficients for 2D modelling on vegetated floodplains. *Hydrological Processes*, *18*(15), 2907–2926. https://doi.org/10.1002/hyp.5596
Wallace, J. M. (2016). Quadrant analysis in turbulence research: History and evolution. *Annual Review of Fluid Mechanics*, *48*, 131–158.
Wallace, J. M., Eckelmann, H., & Brodkey, R. S. (1972). The wall region in turbulent shear flow. *Journal of Fluid Mechanics*, *54*(1), 39–48.
White, B. L., & Nepf, H. M. (2007). Shear instability and coherent structures in shallow flow adjacent to a porous layer. *Journal of Fluid Mechanics*, *593*, 1–32. https://doi.org/10.1017/S0022112007008415
White, B. L., & Nepf, H. M. (2008). A vortex-based model of velocity and shear stress in a partially vegetated shallow channel. *Water Resources Research*, *44*, W01412. https://doi.org/10.1029/2006WR005651
Willmarth, W. W., & Lu, S. S. (1972). Structure of the Reynolds stress near the wall. *Journal of Fluid Mechanics*, *55*(1), 65–92.

Xiaohui, S., & Li, C. W. (2002). Large eddy simulation of free surface turbulent flow in partly vegetated open channels. *International Journal for Numerical Methods in Fluids*, *39*(10), 919–938. https://doi.org/10.1002/fld.352

Zong, L., & Nepf, H. M. (2010). Flow and deposition in and around a finite patch of vegetation. *Geomorphology*, *116*(3-4), 363–372. https://doi.org/10.1016/j.geomorph.2009.11.020